


Review

Back to the Structural and Dynamical Properties of Neutral-Ionic Phase Transitions

Marylise Buron-Le Cointe ¹, Eric Collet ¹ , Bertrand Toudic ¹, Piotr Czarnecki ² and Hervé Cailleau ^{1,*}

¹ Institut de Physique de Rennes, Université de Rennes 1-CNRS, UMR 6251, 263 Avenue du Général Leclerc, 35042 Rennes CEDEX, France; marylise.buron@univ-rennes1.fr (M.B.-L.C.); eric.collet@univ-rennes1.fr (E.C.); bertrand.toudic@univ-rennes1.fr (B.T.)

² Faculty of Physics, A. Mickiewicz University, ul. Umultowska 85, 61-614 Poznan, Poland; pczarnec@amu.edu.pl

* Correspondence: herve.cailleau@univ-rennes1.fr; Tel.: +33-2-2323-6056

Academic Editors: Anna Painelli and Alberto Girlando

Received: 1 August 2017; Accepted: 13 September 2017; Published: 23 September 2017

Abstract: Although the Neutral-Ionic transition in mixed stack charge-transfer crystals was discovered almost forty years ago, many features of this intriguing phase transition, as well as open questions, remain at the heart of today's science. First of all, there is the most spectacular manifestation of electronic ferroelectricity, in connection with a high degree of covalency between alternating donor and acceptor molecules along stacks. In addition, a charge-transfer instability from a quasi-neutral to a quasi-ionic state takes place concomitantly with the stack dimerization, which breaks the inversion symmetry. Moreover, these systems exhibit exceptional one-dimensional fluctuations, with an enhancement of the effects of electron-lattice interaction. This may lead to original physical pictures for the dynamics of pre-transitional phenomena, as the possibility of a pronounced Peierls-type instability and/or the generation of unconventional non-linear excitations along stacks. Last but not least, these mixed stack charge-transfer systems constitute a valuable test bed to explore some of the key questions of ultrafast photo-induced phenomena, such as multiscale dynamics, selective coherent excitations and non-linear responsiveness. These different aspects will be discussed through the structural and dynamical features of the neutral-ionic transition, considering old and recent results, open questions and future opportunities. In particular, we revisit the structural changes and symmetry considerations, the pressure-temperature phase diagrams and conclude by their interplay with the photo-induced dynamics.

Keywords: neutral-ionic phase transition; structural changes; symmetry breaking; Landau phenomenology; dynamical properties; quantum vs. thermal effects; electronic ferroelectricity; P-T phase diagram; photo-induced phase transitions; ultrafast dynamics

1. Introduction

Despite the Neutral-Ionic (N-I) phase transition was discovered a long time ago, and that a large number of progresses have been carried out since through numerous experimental and theoretical works, many key physical features are hand in hand with many today's science topics: Mott physics, electronic ferroelectricity, excitations in one-dimension (1D), light or electric field pulse control, ... The story has begun with the observation, by Torrance et al. in 1981, of a marked color change under pressure of several mixed-stack organic charge-transfer (CT) materials [1], as illustrated by optical microscopy in Figure 1. In contrast with segregated-stack CT crystals giving rise to the well-known family of 1D organic conductors, in the mixed-stack CT crystals electron donor (D) and acceptor (A) molecules alternate along the same stack [2]. A partial degree of charge transfer q , in other words

a partial ionicity, results from the hybridization of the D and A molecular orbitals along stacks with a high degree of covalency: $\dots D^{+q} A^{-q} D^{+q} A^{-q} D^{+q} A^{-q} D^{+q} A^{-q} \dots$ [3]. The color change observed through the N-I phase transition (Figure 1) has been demonstrated to originate from an unusual large increase of the degree of charge transfer, i.e., the ionicity [4,5], from a quasi-neutral molecular state with a low q , stable at low pressure, to a quasi-ionic state with a high q , stable at high pressure. This is in agreement with the gain under pressure in the Madelung electrostatic energy which competes with the ionization cost of a DA pair. In a simple physical picture, a N-I boundary may be defined when the ionicity q crosses a critical value of $1/2$. Actually, the N phase is considered to be a band insulator (nonmagnetic) and the I phase a Mott insulator (magnetic), which originally meets the physics of correlated electrons. In addition, a dimerization process may take place along the mixed stack giving rise to polar DA chains, mainly in the I Mott phase and generally discussed in terms of spin-Peierls instability. Consequently, cooperative inter-stack interactions may drive (anti)ferroelectric ordering phenomena.

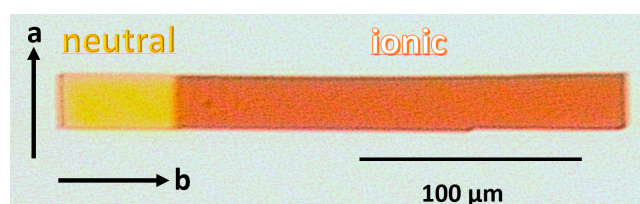


Figure 1. Snapshot of the coexistence of N and I state at T_{NI} manifested in tetrathiafulvalene-*p*-chloranil (TTF-CA) by color changes. Adapted with permission from Reference [6]. Copyright 2003 American Physical Society.

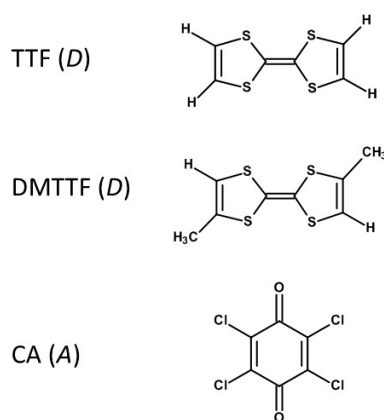


Figure 2. Chemical forms of the donor and the acceptor molecules for the two DA compounds discussed in detail in this review: TTF tetrathiafulvalene, DMTTF dimethyltetrathiafulvalene and CA *p*-chloranil.

Since the discovery of this intriguing phase transition, the main experimental investigations have been focused on the prototypical compound, the tetrathiafulvalene-*p*-chloranil (TTF-CA), where TTF are D and CA are A molecules (Figure 2). At atmospheric pressure, the crystal of TTF-CA transforms on cooling from the N phase to the I one at $T_{NI} \cong 81$ K. In addition, the crystalline structure of I phase exhibits a ferroelectric array of polar dimerized stacks [7]. Other mixed stacks CT crystals exhibiting N-I phase transition have been discovered, with other structural organization, but their number remains quite limited, in particular for those presenting this transition at atmospheric pressure. A wealth of remarkable physical properties observed around the N-I transition provides a particularly original example of the physics of emergent phenomena, which results from complex correlations of

structural and electronic degrees of freedom. This intrinsic richness expresses through different facets. On this point, we can underline some main structural and dynamical features:

- The concomitant totally symmetric charge transfer instability with the symmetry breaking resulting from (anti)ferroelectric ordering leads to an unusual and rich phase transition phenomenology [8];
- The high degree of covalency, with respect to conventional ferroelectric materials, makes these mixed stack charge transfer crystals highly electronically susceptible, and so drives the most spectacular manifestation of electronic ferroelectricity [9];
- The strong 1D fluctuations in the neutral phase [10,11] enhances the effect of electron-phonon interaction. It may give rise to a pronounced Peierls-type anomaly in lattice phonon spectrum and/or the generation of unconventional non-linear excitations along DA stacks, with a puzzling interplay between quantum and thermal effects;
- The groundbreaking observation of the photo-induced N-I instability [12] has opened a way for directing the functionality of these materials by light or electric field pulse on ultra-short time scale.

The goal of this review is to revisit the structural and dynamical properties of typical mixed-stack CT crystals around their N-I transformation. This special issue of *Crystals* illustrates the intrinsic richness of the N-I transformations through a diversity of experimental and theoretical investigations, but with also a diversity of points of view and proposed physical pictures on remaining open questions. This paper is built on the coming back to old and recent established experimental results, bringing out opened questions and future opportunities. Firstly, we want to learn of diverse structural studies to deeply review the two simultaneous key features characterizing a N-I phase transition, the totally-symmetric change of ionicity and the symmetry breaking resulting from the ordering between polar dimerized stacks. This will lay down the foundations for using the universal Landau approach to clarify its singular position in the realm of phase transitions. Secondly, we consider the 1D character and its consequences on dynamical quantum or thermal fluctuations. In the same section, we revisit the pressure-temperature (P-T) phase diagram of TTF-CA through the Landau phenomenology and the relation with the electronic ferroelectricity. Finally, we review in the conclusion the photo-induced phenomena under the light of structural and dynamical properties at thermal equilibrium. In addition, an appendix will give small overview of general concepts involved in the phenomenological Landau theory.

2. Concomitant Totally Symmetric Ionicity Change and (anti)Ferroelectric Symmetry Breaking

Symmetry analysis is a source of valuable insights to investigate the transformation of matter. Thus, the concept of symmetry breaking and order parameter, introduced by Landau, fruitfully provides a universal approach for the analysis of phase transitions, when group-subgroup relationship between the two phases exists. Another great advantage of the Landau theory is the use of a simple potential picture based on the Landau expansion of the relevant thermodynamic potential as a function of the order parameter(s), which provides the simplest approach to discuss the stability, metastability and instability of a system. The validity of this analytic expansion is based on the mean field approximation. However, it is valid in the case of long range electrostatic or elastic interactions, those being particularly relevant in the case of the N-I transition. The Landau theory, summarized in Appendix A, was intensively used in the case of ferroelectric phenomena [13]. However, for the N-I phase transition it is necessary to go beyond the analysis of conventional (anti)ferroelectric systems since, contrary to the polar symmetry breaking, a large change of the degree of charge transfer concomitantly takes place, which per se does not imply a change of symmetry. In other words, this singular phase transition combines two facets, a symmetry breaking one and a so-called isostructural one, i.e., without change of symmetry. This is perfectly illustrated by the main features of structural changes in the TTF-CA prototype compound, overviewed below. The description in terms of Landau

theory for this complex situation requires to consider two kinds of order parameters, the symmetry breaking one and the totally symmetric other one. Thus, every electronic and structural change may be decomposed into two parts, the symmetry breaking one and the totally symmetric one. This may concern electronic redistribution as well as molecular displacements and deformations. The advantage of this phenomenological approach, based uniquely on the universal grounds of symmetry and thermodynamic potential picture, is independent of microscopic details and valid both for thermal and quantum transitions. Beside the microscopic considerations, it offers a different view of the phase transitions.

This complex situation implies two kinds of driving forces, related to the charge transfer instability and the ferroelectric ordering. These have been long-discussed within the frame of theoretical microscopic approaches taking into account electron, spin and lattice degrees of freedom, through correlated electron models [14] and *ab-initio* electronic structure calculations [15,16]. As underlined in [14], the lattice and molecules are particularly “soft”, which is an intrinsic characteristic of a molecular crystal. It is important to underline that the phase transitions take place at 3D and are driven by cooperative electrostatic and elastic inter-stack interactions. They play a key role not only in the (anti)ferroelectric ordering process, but also for the totally symmetric change. Beyond the generally involved spin-Peierls mechanism, the polarization energy gain has to be considered similarly to other ferroelectrics. The strong degree of covalency, manifested through the electronic ferroelectric nature of these charge transfer systems, enhances again more these dipolar interactions. Elastic degrees of freedom manifest through the volume change during the transition which, with the entropy evolution, is essential to describe the thermodynamics of the N-I transition.

2.1. Symmetry Analysis and Structural Changes of TTF-CA

We begin by discussing in TTF-CA the nature of the symmetry breaking (Figure 3), and therefore the nature of the order parameter characterizing this symmetry breaking [7]. At atmospheric pressure, the N phase is thermodynamically stable above $T_{NI} \cong 81\text{K}$. Its space group is monoclinic $P2_1/n$, as determined by the systematic forbidden Bragg reflections $0\ k\ 0$: $k = 2n + 1$, fingerprint of screw axis 2_1 parallel to b , and $h\ 0\ l$: $h + l = 2n + 1$, fingerprint of glide plane n parallel to (a, c) . There are two symmetry related DA pairs in the unit cell with the TTF (D) and CA (A) molecules located on sites with a center of inversion. In each unit cell, the two DA stacks, parallel to the a axis, are regular since non-dimerized. A structural symmetry breaking takes place in the I phase below T_{NI} . There is no change of cell multiplicity, and no change of Bravais lattice. The symmetry lowering manifests in the diffraction pattern by the appearance of weak $0\ k\ 0$: $k = 2n + 1$ Bragg reflections indicating the loss of the screw axis. This necessarily implies the loss of inversion symmetry, in agreement with the observation of a spontaneous electric polarization [8], and in connection with the dimerization process along stacks. By contrast, the glide plane is conserved and it relates the two equivalent DA dimers in the unit cell. The space group of the I phase is then Pn , which is a subgroup of $P2_1/n$, and which is a non-chiral polar group. The order parameter η is therefore scalar (one-component) of B_u symmetry, according to the point-group symmetry C_{2h} ($2/m$) of the N phase. This indicates that in this ferroelectric system the electric polarization lies parallel to the (a, c) plane. Actually, the main component of dimerization displacements is along a , in agreement with the recently observed direction of electric polarization [8]. The intensity of $0\ k\ 0$: $k = 2n + 1$ reflections is directly proportional to the modulus square η^2 of the order parameter. The appearance of new Bragg reflections characterizing a ferroelectric order is rare in respect to conventional symmorphic ferroelectrics, and is a consequence of the non-symmorphic nature of the TTF-CA structure (loss of the screw axis). The structure factor of these new $(0\ k\ 0)$ reflections is proportional to the amplitude of dimerization displacements, but exclusively to the component of displacements along b in accordance with the direction of their scattering wave vector Q_{0k0} . As this component is significantly weaker than the one along a , this explains why these reflections are weak. The temperature behavior of their intensity is abrupt at T_{NI} , exhibiting a large jump. This indicates that this phase transition is strongly first-order.

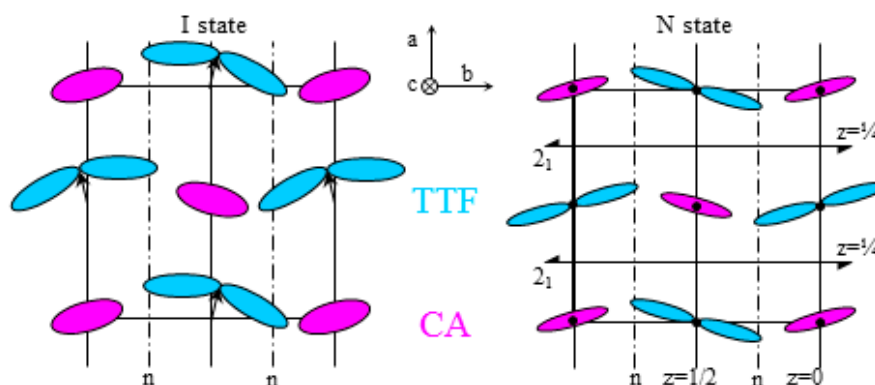


Figure 3. Schematic drawing of the structural changes in TTF-CA from the N ($P2_1/n$) to I (Pn) phase including symmetry breaking and isostructural ones.

The structural changes are not limited to that resulting from this symmetry breaking, since large isostructural variations which respect all elements of symmetry of the N phase are also observed. In other words, these last changes are totally symmetric (A_g symmetry) and may be related to the change of the degree of charge transfer. The evolution of the ionicity in each phase and its jump at the N-I transition was firstly obtained from electronic [5,17] and vibrational [18] optical spectroscopies. This point is extensively reviewed and updated in this NI issue [19,20]. The ionicity q is estimated to be in the range 0.2–0.3 with a slight increase when decreasing temperature in the N phase. It jumps up to about 0.6–0.7 in the I phase. This change may be also estimated on the basis of crystallographic measurements through the variation of some typical bond lengths sensitive to molecular ionicity, such as C=C and C-S in TTF and also C=O and C-Cl in CA [6]. The dependence of the bond lengths and vibrational frequencies on the molecular ionicity of TTF (different oxidation states) has been calculated through a first principles study [21]. Actually, the charge transfer is not really an unambiguously defined quantity since the static charge of an ion depends on how you “count”. Some fundamental reasons why there is not a real relationship between a net static physical charge and the degree of oxidation have been recently discussed for transition metals [22]. The situation is also complex in charge transfer crystals and we will come back later to this point in relation with the electronic ferroelectric properties developed hereafter. However, the topological analysis of the charge density in D and A molecules may provide elaborated information on the degree of charge transfer. Thus, such a critical discussion on the quantification of the intermolecular charge transfer was made using high-resolution X-ray diffraction experiments and the state-of-art density functional theory calculations [23].

As previously underlined, each observed structural changes can be decomposed between a symmetry breaking component proportional to the order parameter η (B_u symmetry) and a totally symmetric part (A_g symmetry) which can be described by another order parameter x (Appendix A). The first one is only non-zero in the phase I, contrary to the second one which can take finite value in each phase. Thus, about the intramolecular deformations, the loss of inversion centers manifests by a dissymmetry of TTF and CA molecular geometries, while the totally symmetric part can be estimated from the modifications of some typical average bond lengths (“molecular volume” by analogy with the spin transition). Different spectroscopies can efficiently probe locally the site symmetry and intramolecular change of D and A molecules. Beside the intramolecular vibrational probes already mentioned, ^{35}Cl Nuclear Quadrupolar Resonance (NQR) provides exceptionally sensitive local probes of CA ($\text{C}_6\text{Cl}_4\text{O}_2$) molecular changes. This allows following the evolution of both symmetry breaking and totally symmetrical changes with temperature (Figure 4) [24–26], as well as under pressure [8]. Since there are two independent Cl in the N phase, two NQR lines are observed. On the one hand, the loss of inversion symmetry leads to the splitting of each of these two lines in the I phase, in accordance with the differentiation of C-Cl bond lengths. On the other hand, the totally symmetric change at T_{NI} is observed through a large frequency jump between a N line and the average frequency of its

corresponding I doublet. Superimposed to the standard evolution of the frequency resulting from regular thermal motions, some pretransitional evolution is observed on both side of T_{NI} [25].

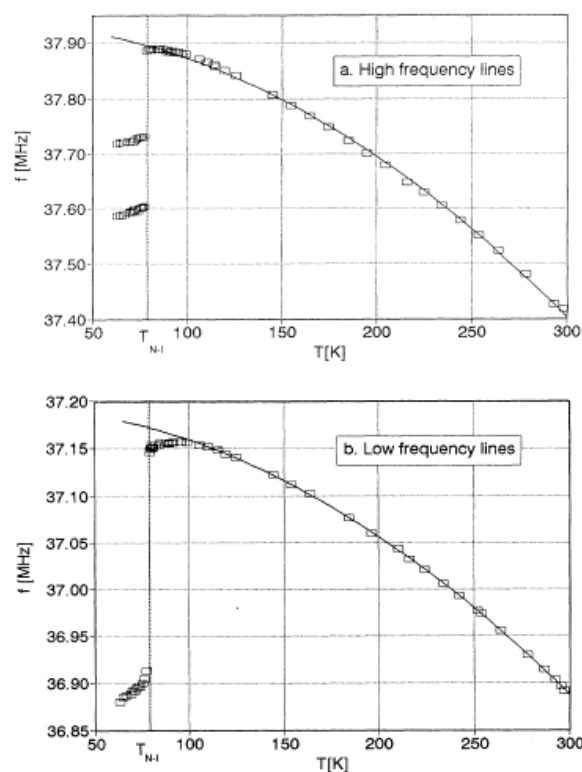


Figure 4. Temperature dependence of the high-(a) and low-(b) frequency chlorine NQR lines in TTF-CA. From Reference [24,25] with permission. Copyright 1993 American Physical Society.

Notice that one of the most characteristic totally symmetric structural changes is provided by the evolution of the unit cell parameters, and consequently of the volume. Indeed, this phase transition is non-ferroelastic, since the same monoclinic crystalline system is kept between the two phases. The stacking axis **a** exhibits a strong contraction when decreasing temperature in the N phase which favors the establishment of the I state in a DA chain by the increasing of the Coulomb energy [26]. No jump is observed at T_{NI} , but only a slight change of the slope in the evolution of this contraction. By contrast, the thermal contraction is weaker for **b**, **c** and β cell parameters than for **a**. However, a jump to smaller values is observed at T_{NI} , and the largest one for **b** ($\Delta b/b \cong 0.5\%$). Therefore, a discontinuous volume contraction occurs at T_{NI} , significant but small. This volume contraction, originating from discontinuous contraction of the unit cell along directions perpendicular to the stacks, leads to a significant Madelung energy gain in the I phase. This can be related to calculations of the Madelung energy, taking into account the intramolecular charge distribution, and which underlines the crucial role of interchain electrostatic interactions [27,28]. In addition, this volume contraction shows that the role of elastic interactions has to be taken into account. Anyway, this observation of volume jump is important to describe the thermodynamics of the neutral-ionic phase transition. In particular, by using the Clapeyron relation for this first-order phase transition, this observation of a $\Delta V \cong 4 \text{ \AA}^3$ per unit cell, combined to the observation of the slope at atmospheric pressure of the transition line in the (P,T) phase diagram $dP/dT \cong 3.6 \text{ MPa/K}$ [8], yields to an entropy jump $\Delta S \cong 9 \times 10^{-23} \text{ J/K}$ per DA pair, in good agreement with the experimental observation [6]. At atmospheric pressure, a large part of the increase of entropy in the N phase is very likely related to a change of the vibrational spectra, the lattice becoming slightly softer in the N phase due to the increase of the unit cell volume.

The first-order nature of the NI phase transition in TTF-CA at atmospheric pressure is unambiguous with the discontinuous appearance of new Bragg reflections, as well as the jump of the cell parameters in the (**b**,**c**) plane. Furthermore, a thermal hysteresis was reported, with a 2 K width by neutron diffraction [6] and about 1 K in an X-ray diffraction experiment using a smaller single crystal [22]. Similar thermal hysteresis was also detected by NQR measurements on crystals of large size [26], as well as electric conductivity [29] and specific heat measurements [30]. In addition, the coexistence of N and I phases is clearly observed by neutron diffraction both on the cooling and heating transformation curves. It exhibits a multi-step transformation in agreement with multi-peak specific heat anomalies [6,30]. Even inside a plateau the coexistence of the two N and I Bragg peaks is observed, which is the fingerprint of the establishment of a microstructure of coexisting phases at large scale and not of intermediate long period ordered structure of alternating N and I stacks. The coexistence regime is sufficiently wide to allow its capture by optical microscopy, as shown in Figure 1. The phase front is sharp and always oriented perpendicular to the **b** axis, which minimizes the cost in elastic stress energy. It was also observed that the progression across the crystal is done by jumps. Notice that all these kinetic phenomena at large scales depend of the crystalline quality of the sample and the cooling (heating) rate. As usual, the width of the observed thermal hysteresis is much smaller than the one expected from mean field Landau description of the multistable regime described in the following sub-section. Moreover, the real-space observation of two energetically equivalent ferroelectric domains in the I phase has been realized by the electro-reflectance method [31]. Their size is about a few hundred μm .

2.2. Landau Description of the N-I Phase Transition in TTF-CA

The Landau description of the NI phase transition in TTF-CA is singular in the sense that two kinds of order parameters, η for the symmetry breaking and x for the totally symmetric change, have to be taken into account. This rich situation differs from both conventional ferroelectrics, such as in perovskite compounds [12], which are only characterized by a symmetry breaking order parameter η , and isostructural phase transitions in the solid state, such as the Mott transition and the spin transition [32], which are only characterized by a totally symmetric order parameter x . Isostructural transitions, where the crystal symmetry is identical in the two phases, are quite analogous with the gas-liquid transition. For the N-I transition, the Landau expansion of the thermodynamic potential, i.e., the Gibbs free energy when the pressure P and the temperature T are the control parameters, corresponds to the sum of two contributions, $\Phi^S(\eta)$ and $\Phi^T(x)$. They are respectively associated with the symmetry breaking and the totally symmetric part, plus cross terms reflecting the coupling of the two transformations. However, in order to better picture their physical meaning, we choose the electric polarization p as symmetry breaking order parameter η , and the ionicity q to express the totally symmetric. Each of them represents a wide set of electronic and structural changes.

As known, the ferroelectric symmetry breaking part only contains even terms and may be written at zero field ($E = 0$) as indicated in Equation (1) (see also Appendix A):

$$\Phi^S(p) = \frac{1}{2}Ap^2 + \frac{1}{4}Bp^4 + \dots \quad (1)$$

In the ferroelectric phase a spontaneous macroscopic polarization, $\langle p \rangle \neq 0$, emerges, which implies a three-dimensional long range polar ordering. On the other side, in the paraelectric state the macroscopic polarization disappears, $\langle p \rangle = 0$. This does not imply the absence of local dimerization, but means no long range ferroelectric ordering.

The Landau description of isostructural phase transitions in the solid state is less common but may also be employed [33] (Appendix A). It can be applied to the neutral-ionic phase transition when we consider only the charge transfer instability decoupled from the ferroelectric ordering. This isostructural instability manifests in the P and T evolution of the q parameter ($0 \leq q \leq 1$), following the evolution of the totally symmetric order parameter $x = 2(q - q_c)$, where $q_c = 1/2$ and $-1 < x < 1$. In this case,

the (P,T) phase diagram is merely composed of a first-order line (phase coexistence) separating the stable N and I phases and ending at a critical point C, as illustrated in Figure 5. We can choose another convenient system of axis (A',H') where the axis A' starts from the critical point (P_c,T_c) tangentially to the first order line and the axis H' perpendicularly (Appendix A). Then, the phase transition line is defined by H'(P,T) = 0 for A'(P,T) < 0. Above the critical point it corresponds to a crossover regime (A'(P,T) > 0) where the systems smoothly transforms from a N to a I state, in an analogous way with the Mott metal-insulator transition. Around the critical point we can write A' = a[(T - T_c) + α(P - P_c)] and H' = a[-α(T - T_c) + (P - P_c)], where α is the slope of the first order line at the critical point (dP/dT)_C. It determines the temperature evolution q(T) at constant pressure P, or vice-versa, and implies to cross the horizontal transition line H' = 0 along an oblique path. The totally symmetric part for the Landau potential may be written (Equation (2)) in a way quite similar to a symmetry breaking situation (see also Appendix A):

$$\Phi^T(q) = \frac{1}{2}A'(q - q_c)^2 + \frac{1}{4}B'(q - q_c)^4 - H'(q - q_c) + \dots \quad (2)$$

The curve q(H'), resulting from the equation of state H' = A'(q - q_c) + B'(q - q_c)³, is monotonous for A' > 0 with an inflection point at H' = 0 and becomes S-shaped for A' < 0, (Figure 5). It should be underlined that this S-shaped behavior is the fingerprint of a positive feedback mechanism (cooperative action) describing a bistable regime. This is known for the thermal evolution of a set of spin crossover molecules coupled by cooperative elastic interactions [32]. This is also observed for the N-I models discussed in [14,34], in particular the toy model which describes the quantum ground state of a set of DA dimers coupled via cooperative Coulomb interactions.

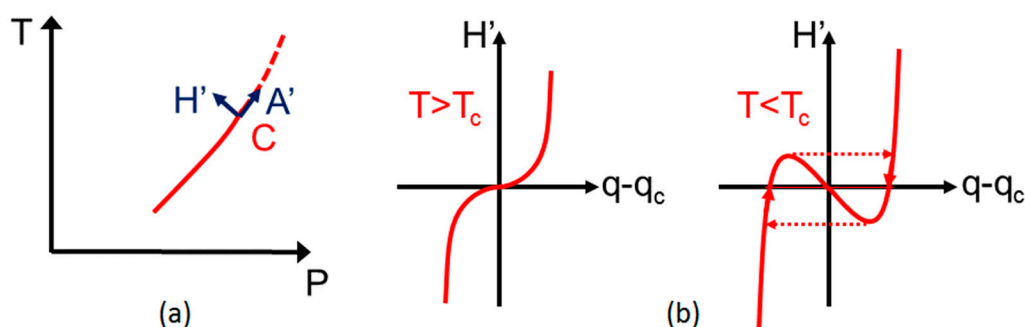


Figure 5. Schematic drawing of the (P,T) phase diagram for an isostructural transition (a) and of the equation of state above (crossover regime) and below (bistable regime) the critical end point C (b).

On the grounds of symmetry considerations, the two first cross terms, expressing symmetry allowed coupling of order parameters (q - q_c) and p, are linear-quadratic and biquadratic, i.e., respectively proportional to (q - q_c)p² and (q - q_c)²p². This approach for determining cross terms is similar to the one used in the analysis by Landau theory of a long-range ordering (η ≠ 0) which emerges in some spin crossover crystals near x ≅ 0 [35]. We can construct these coupling terms on the basis of qualitative physical arguments. Generally, this coupling is only discussed in term of spin-Peierls instability of a regular I stack. In reality, the situation is more complex. Indeed, strictly speaking the term “spin-Peierls” is associated to an ideal pure I state (q = 1). For q = 1/2 this is rather the Peierls instability of a “metallic” state. In addition, beside this Peierls-like mechanism, the dimerization gives rise to a gain in electrostatic polarization energy [36]. Generally, the ferroelectric state is stabilized by an energy term proportional to p² and originating from direct interactions between electrical dipoles (including intra-stack and inter-stack contributions). As the polarization is strongly enhanced by the degree of covalency, which is maximum around q_c = 1/2, one has to introduce a coupling term 1/2μq(1 - q)p², where μ is chosen < 0 in order to stabilize the ferroelectric state. To take into account

the dissymmetry which exists with respect to the spin Peierls-like mechanism, which occurs only in the Mott insulator I state and not in the band insulator N state, we also add another coupling term $1/2\lambda(q - q_c)p^2$ with $\lambda < 0$. Finally, expressing the cross terms as a function of the totally symmetric order parameter, we obtain Equation (3) for the total Landau potential at zero field ($E = 0$), up to the fourth order terms:

$$\Phi(p, q) = \Phi_0 + \frac{1}{2}Ap^2 + \frac{1}{4}Bp^4 + \frac{1}{2}A'(q - q_c)^2 + \frac{1}{4}B'(q - q_c)^4 - H'(q - q_c) + \frac{1}{2}\lambda(q - q_c)p^2 + \frac{1}{2}\mu q(1 - q)p^2 \quad (3)$$

The landscape of the Landau potential is controlled by the P and T thermodynamic parameters which determine the value and the sign of A, A', H', and to a lesser extent B, B', λ and μ . In the discussion below, we will consider these four last ones as constant, and such as B and B' > 0, whereas λ and $\mu < 0$. The coupling term modifies the nature and the temperature where instabilities occur and the phase diagram becomes rich. The stable, unstable and metastable states for a given set of control parameters are obtained with the help of the two equilibrium conditions, expressed in Equations (4) and (5):

$$\frac{\partial \Phi}{\partial p} = Ap + Bp^3 + \lambda(q - q_c)p + \mu q(1 - q)p = 0 \quad (4)$$

$$\frac{\partial \Phi}{\partial q} = A'(q - q_c) + B'(q - q_c)^3 - H' + \frac{1}{2}\lambda p^2 + \frac{1}{2}\mu(1 - 2q)p^2 = 0 \quad (5)$$

In addition to the trivial solution $p = 0$, the Equation (4) exhibits two equivalent non-zero solutions $\pm p$ only if $A + \lambda(q - q_c) + \mu q(1 - q) < 0$. Thus, if the term $\lambda(q - q_c)$ is sufficiently dominant, the emergence of the symmetry breaking requires a sufficiently large “ionicity”, which is effective in I state. This is consistent with the existence of a region in the control parameter space (P-T), where multistability occurs with the presence of three minima: on the one hand a paraelectric N phase with $q < q_c$ and $p = 0$, on the other hand two equivalent ferroelectric I phases with $q > q_c$ and $\pm p \neq 0$. The energy gain provided by the ferroelectric ordering in the I state pushes the N-I boundary at higher temperature with respect of the simple isostructural case. Given the large number of parameters, numerical calculations for a chosen set of parameters allow to visualize the thermodynamic potential landscape (Figure 6). This multistable regime takes place in a 2D order parameter space, which is fundamentally different from the well-known triple-well picture in a 1D order parameter space used for describing a symmetry breaking first-order phase transition when $B < 0$ (Appendix A). It is similar to the one discussed in term of potential energy surface for the ground state of a modified Hubbard model of a mixed DA stack [37], but also in terms of free energy for a simplified model [38]. A similar situation exists in another ferroelectric system, $\text{Sn}_2\text{P}_2\text{S}_6$, and with the same lowering of symmetry as TTF-CA, from $P2_1/n$ to Pn [39]. It has been discussed in term of a strong linear-quadratic interaction between a zone-center fully symmetrical A_g structural distortion and a polar B_u one. In addition, significant coupling between the ferroelectric order parameter and strain is pointed out. As discussed in Appendix A, a coupling term between the totally symmetric strain tensor, describing the volume change, and the ferroelectric order parameter is linear-quadratic by symmetry. This can lead to an evolution of the strain proportional to the square of the order parameter. However, with regard to the essential role of the isostructural change within the N-I transition, a bilinear coupling term between the totally symmetric strain tensor and the totally symmetric order parameter has also to be taken into account.

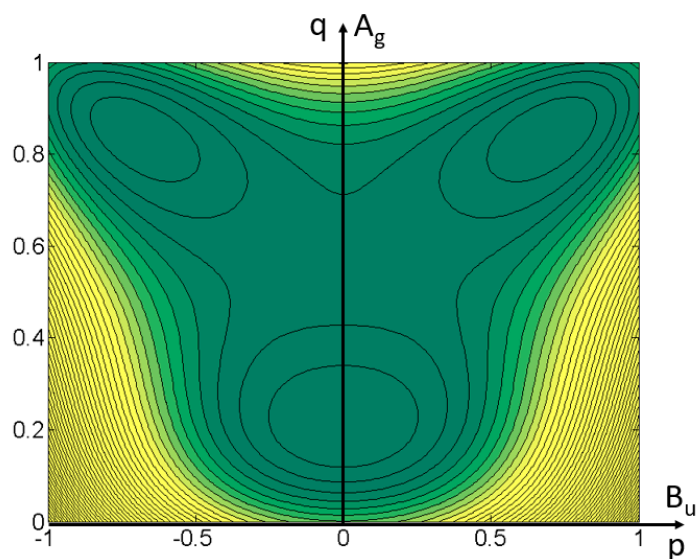


Figure 6. Schematic drawing of the Landau potential energy isolines in the 2D order parameter space around T_{NI} (multistable regime).

Finally, it is interesting to consider the connections with models in statistical physics. It is well known that the situation of symmetry breaking can be described in the simplest way by the famous Ising model, as well as isostructural transitions by a lattice-gas model, actually isomorphous to the Ising model. It was proposed [40–42] to describe the NI transition where the two aspects are combined by the Blume-Emery-Griffiths model [43,44]. The three states, i.e., the non-dimerized N one and the two dimerized I ones, are so described by a spin-1 local variable $S^z = 0 \pm 1$. Therefore, both the ferroelectric ordering $p = \langle S^z \rangle$ and the “ionicity” $q = \langle (S^z)^2 \rangle$ can be obtained from the same Ising variable. In other words, the two facets of the NI transformation can be viewed as that resulting from the condensation and the crystallization of charge-transfer excitations [8]. It is obvious that the Ising approach is only thermal and quantum effects are not included, although essential [45]. Therefore, quantum Monte Carlo method has been used to model the N-I transition taking into account both thermal and quantum phenomena [46].

2.3. Other Examples of N-I in Different Mixed Stacks Charge Transfer Crystals

Some other mixed stack charge-transfer crystals exhibit NI or related phase transitions, but their number remains limited. The comparison of their structural properties with the one of the prototypical compound TTF-CA is instructive, especially when the characteristic of the phase transition and/or the nature of the symmetry are different. In this review about structural and dynamical properties we mainly focus on the case of the dimethyltetrafulvalene-*p*-chloranil (DMTTF-CA) [47] which presents two key physical features different from TTF-CA: a cell doubling in the ordered I phase and a quasi-continuous transition [48]. Despite being close to TTF-CA in the nature of their DA molecular pairs, the structural organization is quite different. Thus, the high-temperature phase is triclinic $P\bar{1}$, with only one DA pair by unit cell, included in regular stacks directed along **a**. At $T_c \cong 65$ K, a phase transition takes place and is manifested by the appearance of superstructure Bragg peaks at the zone boundary $\mathbf{k}_c = \frac{1}{2} \mathbf{c}^*$, the Z point of the Brillouin zone. This is the direct signature of a cell doubling along the **c** axis. The nearly second-order nature of this phase transition is established from the observation of a quasi-continuous evolution of the intensity of these superstructure reflections (Figure 7). If the cell doubling necessarily leads to the disappearance of at least one over two inversion centers in the N unit cell, the total disappearance of all inversion centers is more difficult to establish. It explains the difficulty to choose between an antiferroelectric structure ($P\bar{1}$) corresponding to an antiparallel array along **c** of polar planes in the same ionicity state, and a ferroelectric one ($P1$) with an ionicity

which differs between the two kinds of polarized planes [48–50]. The antiferroelectric situation is more natural when we consider the Landau analysis. Indeed, in the ferroelectric scenario the anti-ferroelectric order parameter has to be coupled through a biquadratic crossing term to another order parameter corresponding to the alternation of ionicity, and so involving another irreducible representation at the Z point. In this situation, a second-order phase transition emerges only at a single point of the control parameter space [51]. In addition, some first-principles DFT calculations support the scenario of similar ionicity in the two kinds of polarized planes [52]. It is interesting to remark that, contrary to antiferromagnetism, the antiferroelectricity is often considered as ill-defined [13], due to the absence of specific symmetry properties to characterize an anti-polar ordering in a nonpolar phase. Some more elaborated criteria allowing to make the definition of antiferroelectricity clearer, such as a local symmetry-breaking mechanism defining polar sites have been recently proposed [53]. With regard to its intrinsic simplicity, DMTTF-CA offers a nice illustration of this proposed physical picture. The polarization p is coupled to the order parameter η , which characterizes the translational symmetry breaking, through a biquadratic cross term $1/2\delta\eta^2p^2$. This coupling term determines the responsiveness of the system to an external electric field. For $\delta > 0$, it drives a decrease of the dielectric permittivity as observed in DMTTF-CA [10].

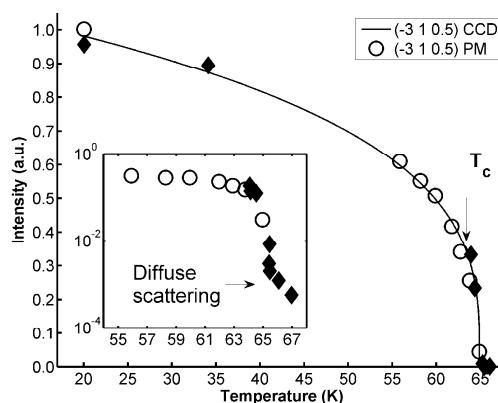


Figure 7. Temperature evolution of the superstructure reflection intensity in DMTTF-CA measured by X-ray scattering. The insert shows the intensity measured at maximum with a high-resolution.

This anti-ferroelectric structural organization is strongly supported by ^{35}Cl NQR measurements, which directly probe the symmetry change of Cl sites [54]. Below T_c , and for each NQR lines of the N phase, a splitting in only two lines is observed, showing that a center of inversion is kept in the unit cell. In addition, the relative temperature dependence of the order parameter can be obtained looking at the frequency splitting of each line which is proportional to η . By fitting the experimental value with a power law $\eta \sim (T_c - T)^\beta$, a low critical exponent is obtained: $\beta \cong 0.16$. This is probably an indication that the phase transition is weakly first-order, being close to a tricritical point. Indeed, it is known that in such situation the evolution of the order parameter can artificially be fitted by a power law with $\beta = 1/6$ [55]. It is confirmed through a high-resolution X-ray scattering measurement of the superstructure peak. Its evolution is compatible with a very small jump of the order parameter at the transition temperature (Figure 7). Moreover, the average frequency shifts are smaller than the ones observed in TTF-CA indicating so a smaller ionicity change. A detailed vibrational spectroscopic investigation of DMTTF-CA confirms a quasi-continuous evolution of the ionicity when crossing the phase transition, but its increase in the low temperature phase remains more limited than in TTF-CA, with a value remaining below $q_c = 1/2$ [56]. Therefore, it was proposed that the ionicity remains always below the N-I boundary, i.e., on the N side in the low-temperature phase. This situation where the N-I boundary is not crossed is fundamentally different of the one in TTF-CA. It may appear in other mixed stack compounds, as for instance in TMB-TCNQ [57]. Strictly speaking, the phase

transition in DMTTF-CA is no more a true N-I transition, and the anti-polar ordering process becomes the relevant driving force. This may be expressed in the Landau expansion in a similar way to TTF-CA by a crossing term proportional to $\alpha q(1 - q)\eta^2$, with $\alpha < 0$, to take into account that the anti-polar interactions may also be enhanced by charge fluctuations, and not the spin-Peierls mechanism. This is certainly an important key to understand the difference of behavior in DMTTF-CA by comparison with that of the prototype TTF-CA. At the transition temperature the ionicity q_0 is small compared to 1, and consequently the coupling term simplifies in $\alpha q\eta^2$, in a first approximation. Additionally, because the system is far from the NI instability, we may consider a restoring force for the ionicity by adding a quadratic term $1/2K(q - q_0)^2$, where K , related to A' , is > 0 (q_0 is also depending of H'). Therefore, the Landau expansion limited to simple relevant terms becomes (Equation (6)):

$$\Phi(\eta, q) = \Phi_0 + \frac{1}{2}A.\eta^2 + \frac{1}{4}B.\eta^4 + \frac{1}{2}K(q - q_0)^2 + \alpha q\eta^2 \quad (6)$$

The situation is totally identical to the one encountered by the coupling with a totally symmetric strain deformation discussed in Appendix A, and so $q - q_0 = -(\alpha/K)\eta^2$. This appears quite compatible with the NQR observations of the spectral shift, probing the q evolution [53]. Moreover, the absence of the isostructural N-I instability makes that this transition may be continuous or quasi-continuous, since this suppresses the possibility of a three-well potential in a 2D order parameter space as in TTF-CA (Section 2.2). This kind of coupling also introduces the possibility of a three-well potential, but in the 1D order parameter space for η , and so of a tricritical point.

Additional mixed stack compounds are discussed in another paper of this special issue on N-I transition [18]. Here, we focus on some examples close to TTF-CA and DMTTF-CA. Thus, in the TTF complex with QBrCl_3 , where a chlorine is replaced by a bromine, a temperature-driven N-I phase transition takes at lower temperature (68 K) than in TTF-CA and with very similar structural properties [58]. In contrast, the TTF-BA, tetrathiafulvalene-*p*-bromanil, presents a structural array totally different with an unusual crystal packing composed of two quasi-orthogonal mixed stacks [59,60]. A ferroelectric phase transition takes place at 53 K, with a space group change from $P\bar{1}$ to $P1$ without change of cell multiplicity. It is associated to a dimerization process originating from the loss of inversion centers. The mixed stacks are practically completely ionized in both phases, with their ionicity in the range 0.95–1, which does not significantly change at the transition. In the high-temperature phase the system is paramagnetic, in agreement with a Mott insulator state, and it was suggested that the transition is driven by the spin-Peierls instability [61]. Moreover, an interesting series of CT complexes, isomorphous to DMTTF-CA by successive replacement of chlorine by bromine on the A molecule, has been studied in order to investigate a quantum paraelectric state [62,63]. These different observations illustrate the wide variety of situations. They also show that a chemical substitution may considerably change the nature of N-I transitions.

Finally, we would like to mention two intriguing situations in compounds not close to TTF-CA. Thus, the (BEDT-TCNQ)-(CIME-TCNQ) presents a neutral-to ionic phase transition only under pressure [64] and where the space group $P2_1$ of the N phase is already non-centrosymmetric. It is a chiral and polar group, with a polarization parallel to the screw axis 2_1 . Crossing the transition under pressure gives rise to a symmetry breaking with the establishment of the space group $P1$. The second case concerns a metal-complex-based covalently bonded DA chain compound, beyond stacked π -DA charge transfer systems. It presents stepwise N-I phase transitions [65], with an intermediate phase between a high temperature N phase fully neutral with and a low-temperature I phase fully ionic, in the temperature range $210 \text{ K} < T < 270 \text{ K}$. This phase is characterized by an average ionicity of about 1/2 and a long range ordering between N and I chains, in relation with the appearance of superstructure reflections.

3. Electronic Ferroelectricity, Fluctuations and Self-Ordering of a Set of DA Chains

After having developed in the part 2 symmetry analysis and Landau approach on the grounds of structural features, this part 3 focuses on the important key microscopic mechanisms governing the fascinating properties around the N-I transition. On the one hand, it is important to make the link with the recent observation of electronic ferroelectric properties in TTF-CA [9]. The enhancement of the spontaneous electric polarization by covalency is spectacular, with an electronic contribution to the polarization which is much larger than the one due to the displacement of molecular ions with static charge, and above all which is in the opposite direction counterintuitively. A number of theoretical works supports this remarkable manifestation of electronic ferroelectricity [14,66,67]. On the other hand, it is also important to underline that the pre-transitional fluctuations which develop in the N phase on approaching the N-I instability are strongly 1D [10,11]. This is particularly true in TTF-CA, for which no inter-stack correlations are observed even close to the N-I transition. Therefore, this N phase may be described as a set of weakly coupled DA chains. This exceptional 1D character of the N phase gives rise to remarkable dynamical features such as the possibility of a pronounced Peierls-type anomaly in the lattice phonon spectrum and/or the generation of non-linear excitations, i.e., moving kinks separating N and I strings along the chain. However, in addition to these 1D physical features along DA chains, the inter-chain coupling is essential to drive the phase transition toward the I phase. Finally, we will revisit the (P,T) phase diagram [8], including some dielectric measurements bringing new information on the unconventional ferroelectric behavior of TTF-CA. Generally, the interplay between quantum and thermal fluctuations is at the heart of the quasi-unique physical properties of NI systems.

3.1. Electronic Ferroelectricity of TTF-CA

In connection with the first feature concerning electronic ferroelectric properties, it is interesting to underline that, in classical solid-state physics textbooks, the emergence of a permanent spontaneous electric polarization is generally described as purely originating from the relative shifts of point charged ions within the non-centrosymmetric structure (ionic ferroelectricity). This physical picture is too naive since there is a significant enhancement of the polarization by an additional electronic contribution associated to the redistribution of electrons [68]. To deal with this effect, an effective charge, named the Born effective charge Z^* , is ascribed to each ion and defined by the first derivative of polarization with respect to atomic displacements. The modern Berry-phase theory of polarization states that the polarization is a quantum phenomenon, taking into account the delocalized nature of valence electrons [69–72]. Actually, the polarization is not a physical observable and it is always the polarization difference which is measured through dielectric permittivity and ferroelectric hysteresis. This polarization difference is equivalent to a current directly accessible in quantum theory as a property of the phase of the wave-function, as opposed to the charge, which is a property of the modulus. Actually, instead of the static charge of an ion, the Born effective charge, which is well-defined dynamically and measurable, is the relevant physical quantity in order to describe electronic ferroelectricity. In other words, it is not the amount of covalency that is relevant but the change in covalency during ionic displacements.

In conventional ferroelectric crystal, such as the typical example of barium titanate (BaTiO_3), the electronic ferroelectricity part is significant but on the same order of magnitude than the ionic one and their respective polarization points in the same direction. For TTF-CA the ferroelectric hysteresis has been carefully measured [9] much later than the structural studies which evidenced the polar nature of the I phase, because its significant conductivity has long hindered the experimental observation of the spontaneous polarization value. The observed parallelogram-like hysteresis loop allows to demonstrate that the spontaneous polarization, directed along the stack direction \mathbf{a} , is quite large. The measured remanent polarization, very close to the saturated polarization, reaches $6.3 \mu\text{Ccm}^{-2}$ at $T = 59 \text{ K}$. A close value of $6.7 \mu\text{Ccm}^{-2}$ at 56 K is obtained in the derivative TTF-QBrCl₃, which, as mentioned in Section 2.3, exhibits very similar electronic and structural properties with TTF-CA. In contrast, the

polarization in TTF-BA is much smaller, $\sim 0.15 \mu\text{Ccm}^{-2}$ at low temperature [61], in agreement with first-principles calculations of the electronic structure [73]. We can argue that this quasi-fully-ionic compound remains far from the N-I boundary, which greatly reduces the covalency effect. Moreover, the quasi-orthogonal structural array between the two independent mixed stacks introduces an additional reduction. In TTF-CA, the dipolar moment per unit cell is $5.2 \times 10^{-29} \text{ Cm}$, which is more than 20 times greater than the value estimated from a point charge model [7,23]. In another way, the estimation of the Born effective charge is $Z^* = 13.9$, much larger than the estimated charge transfer q of about 0.6–0.7. Above all, the spontaneous polarization counterintuitively establishes in an opposite direction to what the ionic displacements would predict. This latter result was demonstrated thanks to complementary synchrotron diffraction measurements, taking advantage of anomalous X-ray scattering which allow discriminating between the Bragg intensity of the two different ferroelectric domains. These two features, the huge electronic enhancement and the opposite direction for the polarization, make TTF-CA the most spectacular representative of genuine “electronic ferroelectricity”.

The effect of strong electron correlation on electronic ferroelectric properties is essential [74–76], since the I phase is considered to be a Mott insulator (magnetic), while the N phase a band insulator (nonmagnetic). Resta and Sorella have done a general study of such generalized Mott-like transition in a partially ionic insulator, i.e., a mixed covalent/ionic insulator, emphasizing in a remarkable way the difference between static and dynamical charges [77]. Thus, it was shown that in the highly correlated regime, the Mott insulating I state, the anion transports a positive dynamical charge, and the cation a negative dynamical one. Another case of a counterintuitive sign of the dynamical charge has been recently reported in a transition metal system [78]. A detailed analyze for the specific case of the N-I transition is made in the theoretical paper of this *Crystals* issue [14]. The electronic polarization is computed as a Berry phase [79–81]. The sign of charge flux, i.e., the partial derivative of the polarization with the ionic displacement amplitude, switches from negative to positive from the N-to-I side. Another consequence is the highly electrically susceptible behavior around the N-I boundary, where the great electron delocalization drives large charge flows. It is important to underline that *ab-initio* calculations have also predicted the directional change of the total polarization [66,67]. TTF-CA was considered as an organic multiferroic due to the coexistence of ferroelectric and magnetic ordering. Actually, this term “multiferroic” is used in a generalized way, since this is not a ferromagnetic ordering giving the possibility to change the ferroelectric properties by a magnetic field, but the formation of DA pair dimers in a singlet state driven by a Peierls-like mechanism. Moreover, a recent analysis of the covalency effect on polarization with the help of localized Wannier orbitals compare the difference between the organic TTF-CA and typical ferroelectric perovskites [82,83]. There is a fundamental difference in the energy level diagram near the Fermi level between the two cases, which leads to an opposite effect on the electron transfer by pairing. This will be interesting to explore this seductive physical picture in connection with the above discussion. Finally, we would like to underline that the proposed coupling term used in (3), proportional to $q(1 - q)$, is consistent the electronic ferroelectricity picture (maximum of charge fluctuations at $q_c = \frac{1}{2}$).

3.2. One-Dimensional Correlated Fluctuations

One of the most important key feature of mixed stack charge-transfer crystals exhibiting a N-I transition is the fact that their fluctuations in the high-symmetry N phase exhibit pronounced 1D correlations, as directly probed by X-ray diffuse scattering experiments. Indeed, in addition to Bragg diffraction, which probes only the long-range order, there is also diffuse scattering which probes the spatial correlations of local deviations characterizing the short-range order [84]. The spatial extensions of correlations govern the shape of diffuse scattering. Thus, 1D correlated objects manifest via diffuse planes in the reciprocal space, and its spatial extension, the correlation length, can be extracted from the inverse of the width of these diffuse planes. For TTF-CA, diffuse planes perpendicular to the stacking axis \mathbf{a} are observed above T_{NI} [11]. These planes are localized around integer values of the Miller index h , except for $h = 0$ (Figure 8). It constitutes the direct proof of the emergence in the N

phase of strong correlations along DA stacks. On approaching the transition, there is no significant evolution of the intensity modulation inside the diffuse plane and the fluctuations keep their 1D nature. Therefore, the inter-stack correlations are practically non-existent, so the N phase of TTF-CA can be described as a set of independent DA chains, while the discontinuous establishment of 3D long range order in I phase below T_{NI} requires 3D inter-stack cooperativity. It should be underlined that this 1D character is really pronounced, even more than in molecular conductors [84]. The X-ray diffuse scattering in reciprocal \mathbf{k} -space directly probes the spatial extent of time-averaged correlated fluctuations, $\langle p(\mathbf{r})p(0) \rangle$ and $\langle q(\mathbf{r})q(0) \rangle$, through its intensity $I(\mathbf{k})$ which is proportional to the weight of their respective Fourier components $\langle |p_{\mathbf{k}}|^2 \rangle$ and $\langle |q_{\mathbf{k}}|^2 \rangle - \langle q_{\mathbf{k}} \rangle \langle q_{-\mathbf{k}} \rangle$ ($\langle p_{\mathbf{k}} \rangle = 0$ in the N phase). Actually, in relation with the fluctuation-response theorem, these fluctuating Fourier components may be related to a response function, a generalized susceptibility $\chi(\mathbf{k})$, for instance $\langle |p_{\mathbf{k}}|^2 \rangle = k_B T \chi_p(\mathbf{k})$. The behavior of $\chi(\mathbf{k})$ is related to the thermodynamic restoring forces for each order parameters p and q . When q is not too close to q_c , which is valid in a rough approximation for the N phase, the two correlation lengths ξ_p and ξ_q becomes similar [10]. For a set of independent stacks, characteristic of the N phase in TTF-CA, we can only define the correlation lengths along the stack direction \mathbf{a} . Since the variation of the diffuse scattering intensity along \mathbf{a}^* has a Lorentzian shape, corresponding to an exponential spatial correlation decay, from which the 1D correlation length therefore can be extracted. It increases from about 3 DA pairs at 200 K to about 10 pairs near T_{NI} . Moreover, the extremely weak diffuse scattering for $h = 0$ is the indication that the molecular displacements, involved in these pre-transitional correlated fluctuations, are essentially parallel to the stacking axis \mathbf{a} . The nature of these fluctuations is again the object of a controversial debate, and two limit physical pictures exist.

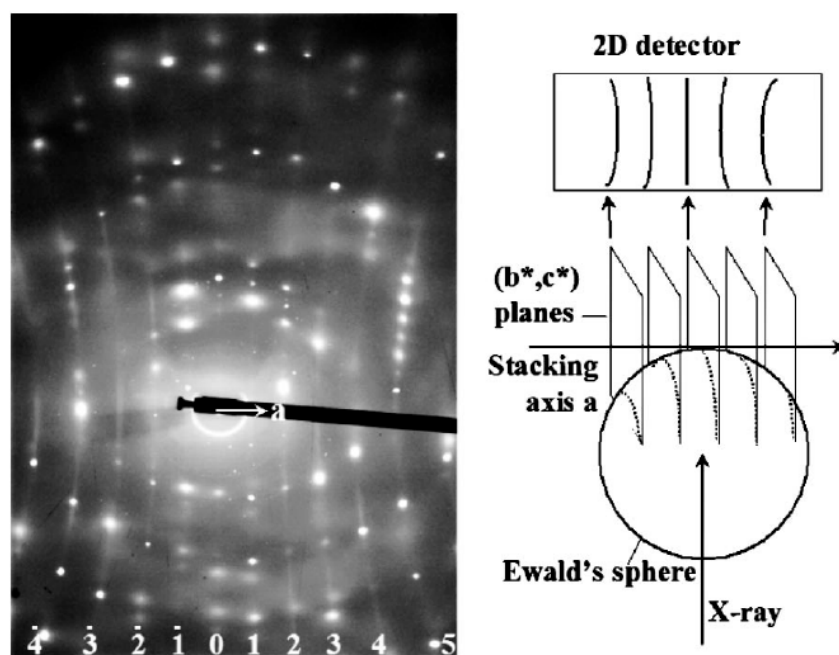


Figure 8. Diffuse planes observed at $T_{NI} + 2K$ (left). The stacking axis \mathbf{a} is horizontal and the projections of the intersection of (b^*, c^*) planes with the Ewald sphere correspond to the diffuse curves (right). From Reference [11] with permission. Copyright 2006 American Physical Society.

First, as suggested in the early time after the discovery of the N-I phase transition, there is the so-called N-I domain-wall picture [85–89]. In the N phase, the DA stacks are considered as inhomogeneous, because of the thermal excitation of fluctuating 1D dimerized I domains at nanoscale, separated from the predominant undimerized N medium by moving N-I domain-walls. These domain-walls are 0D objects (kinks) and must not be confused with neither 2D phase fronts in the

coexistence regime around T_{NI} , nor the 2D domain-walls between ferroelectric domains below T_{NI} . Their dynamical time-scale is also quite shorter than those of slow 2D walls. The thermal excitation of these 1D I nanodomains may become significant when approaching the N-I transition, where the energies of N and I states, or more precisely their chemical potential, becomes close, and so their excitation energy is governed by the domain-wall energy E_{DW} . In addition, the activation of a weak a_g band, observed in infra-red spectrum of the N phase of TTF-CA [90] and the similar TTF-QBrCl₃ [56], has been interpreted as resulting from the local loss of inversion symmetry in dimerized nanodomains. The concentration of dimerized I species in TTF-CA is estimated to about twenty percent on approaching T_{NI} [87]. Moreover, a high reflectance band is observed just above T_{NI} in the far-infrared optical response of TTF-QBrCl₃ [91]. The deduced optical conductivity spectra exhibit a broad absorption band, which shifts at lower energy with increasing spectral intensity when temperature decreases. Finally, an intense peak appears at $\approx 10 \text{ cm}^{-1}$ near T_{NI} . This low-energy excitation was ascribed to the N-I domain-wall dynamics.

Second, there is the soft mode description associated with a pronounced Peierls-like anomaly in the lattice phonon spectrum [92]. It is based on a theoretical description of the N-I transition as a quantum phase transition in a soft lattice controlled by the variation of cell parameters with temperature [14]. The involved B_u soft lattice mode in the N phase of TTF-CA is located at the Brillouin zone-center and, being polar and at low-frequency, it should be detectable in the far-infrared range. However, the low-frequency spectrum is complex and difficult to interpret. Actually, a first indication of a soft mode was discussed in the spectral region of intramolecular vibrations thanks to the observation of sidebands interpreted as combination between totally symmetric vibrations and the soft lattice mode [93]. The frequency of the soft mode was derived from these measurements. It largely decreases from about 70 cm^{-1} at room temperature to about 20 cm^{-1} at T_{NI} . Notice that the interpretation of these additional bands totally differs from the one described above to support the domain-wall picture. A careful and advanced multi-mode analysis of the low-frequency infra-red spectrum [94–96], detailed in [20], indicates an effective pronounced softening, which impressively follows the previous determination from sideband observation. It might be considered as a strong support to the soft mode scenario. This mode becomes overdamped on approaching T_{NI} and an increase in the reflectivity toward zero frequency is observed. The experimental spectral observation present large similarities with the one in TTF-QBrCl₃ reported above, but with a completely different interpretation.

We can discuss the diffuse scattering observations with respect to these two scenarios. In the domain-wall picture, the correlation length, of about 10 DA pairs near T_{NI} , determines the average size of the thermally excited I nanodomains in the N stack, and the domain-wall energy is of the order of thermal energy at ambient temperature [11]. Some theoretical calculations points that the thermal activation of such nanodomains is negligible [37]. Anyway, even if a value of 20 percent of I species is probably excessive, this scenario cannot be completely excluded. In the Peierls soft mode picture, the fluctuations may be expressed in terms of mean-square displacements $\langle |u_k|^2 \rangle$ inversely proportional to ω_k^2 , i.e., to the restoring force in classical approximation. When crossing a diffuse plane perpendicular to \mathbf{a}^* , $I(\mathbf{k}_x)$ is proportional to $k_B T / (\omega_0^2 + \alpha k_x^2)$, where α traduces the wave vector dispersion of the Peierls mode (implicitly there is not dispersion in direction perpendicular to stacks). Following this scenario, as discussed in [11], the dispersion is abnormally large, about $1600 \text{ THz}^2 \text{ \AA}^2$. However, in [92], it was argued that the particularly important electron-phonon coupling in NI systems are able to reproduce such a pronounced Peierls anomaly. In the absence of energy analysis of the diffuse scattering, it is not possible to definitely conclude. In addition, it is quite important to mention that these two scenarios correspond to two limit cases and the real situation may be more complex. Similarly to the well-known interplay between order-disorder and displacive mechanisms in structural phase transitions, an intermediate situation may be considered with the coexistence in the spectral response of a lattice vibrational mode, which partially softens and is less disperse than in the Peierls picture, and a central relaxational one, which can diverge [97,98]. It is also clear from the pictures of potential energy surface, for the ground state [14] as well as the thermodynamic potential (Figure 6),

that, in addition to the coupling between B_u and A_g modes, anharmonic effects can become enhanced on approaching T_{NI} .

The two key differences of DMTT-CA with TTF-CA, its quasi-continuous nature and the cell doubling associated to a zone-boundary critical wave vector $\mathbf{k}_c = \frac{1}{2} \mathbf{c}^*$, leads to a different feature in the diffuse scattering behavior (Figure 9) [10]. Well above the N-I transition diffuse planes are observed, indicating 1D fluctuations. When approaching the transition temperature, a significant modulation of the intensity within the diffuse scattering planes takes place in direction perpendicular to the stacking axis \mathbf{a} , manifesting the establishment of inter-stack correlations. The condensation of this diffuse scattering into a Bragg peak at the zone boundary \mathbf{k}_c , when the 3D long-range order $\langle \eta \rangle \neq 0$ establishes, is clearly observed (Figure 9). As in TTF-CA, a mode softening has been reported by the observation of combinational sidebands [56]. Another interesting feature is the observation of a doublet structure for the C=O and C=C stretching modes in the low-temperature phase and near T_{NI} , suggesting the presence of two slightly different ionized species before the establishment of a complete order at lower temperature. This may constitute an indication that the pure displacive physical picture is not sufficient.

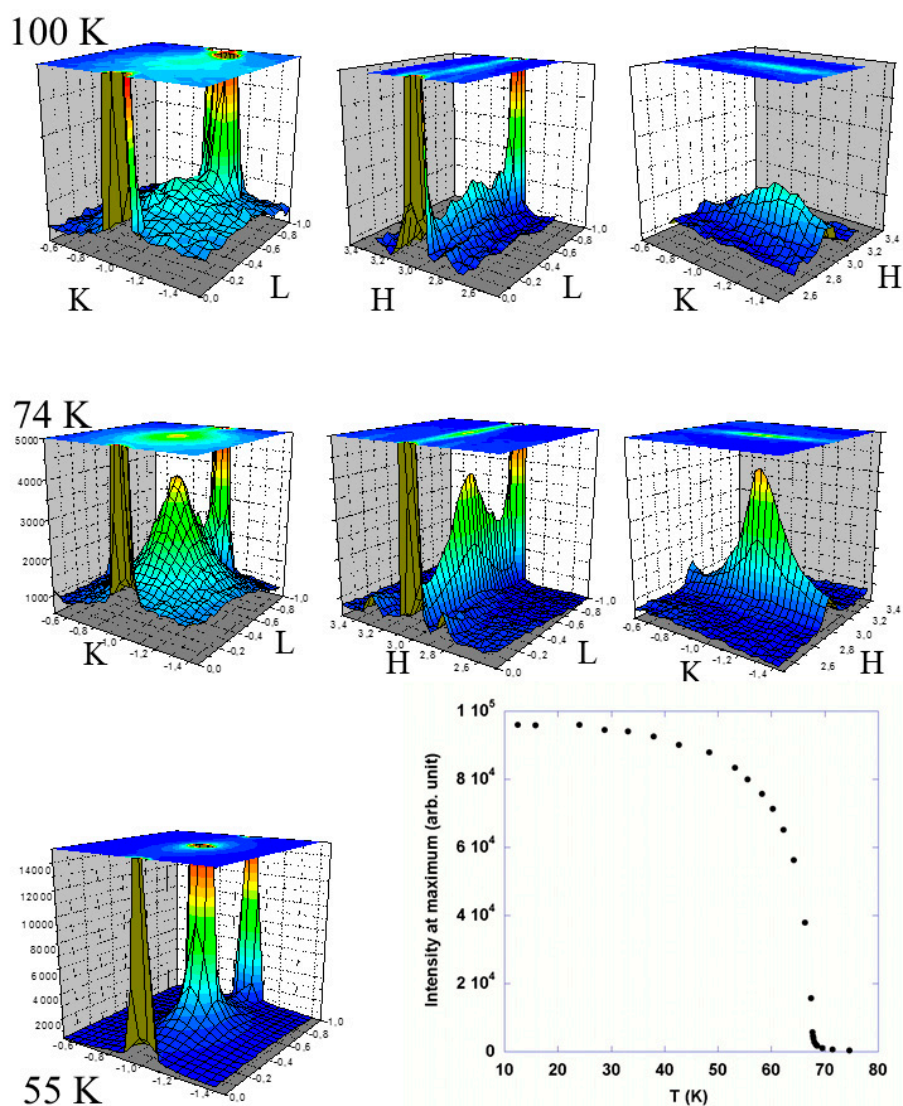


Figure 9. Condensation of the diffuse scattering into a Bragg peak in dimethyltetrathiafulvalene-*p*-chloranil (DMTTF-CA).

3.3. Revisiting the Phase Diagram of TTF-CA and Observation of Electronic Ferroelectric Fluctuations

Pressure is known as playing a central role to control the N-I transition since its discovery [1]. On the one hand, the lattice compression resulting from the application of pressure modifies the interbalance between the gain in Madelung electrostatic energy and the ionization energy cost of a DA pair. Therefore, the I state is favored at high pressure. In addition, the hybridization of D and A molecular orbitals may also be modified. On the other hand, thermal effects have also to be taken into account for a real description of the thermodynamics of the N-I transformation at high pressure where the transitions temperatures largely increase. There are diverse indications of the occurrence of charge transfer thermal fluctuations under these thermodynamic conditions. These points will be discussed below in connection with the thermodynamics of the N-I transition viewed as condensation and crystallization of charge transfer fluctuations [8] and electronic ferroelectric properties.

The phase diagram of TTF-CA is shown in Figure 10. We begin by discussing the experimental results before considering their implications on the physical features of this peculiar phase diagram. Whether they have been performed by neutron diffraction, NQR or dielectric measurements, they have been obtained with well-controlled pressure at different temperatures. Helium gas was employed as the pressure-transmitting medium for this soft molecular material. Single crystal (neutron, dielectric) or a set of small crystals (NQR) are implemented in a pressure cell inside a cryostat, allowing for external control of gas pressure. Therefore, this experimental pressure method is accurate, even when the temperature changes. In the contrary, in diamond-anvil cells or clamps substantial changes of pressure occur with decreasing temperatures.

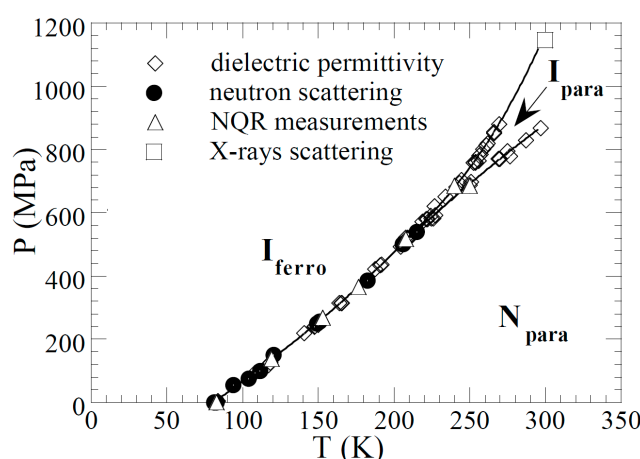


Figure 10. Phase diagram of TTF-CA.

An important feature of the N-I phase transition in TTF-CA is that it becomes less and less discontinuous with increasing pressure. It is revealed by the evolution of the intensity of a typical superstructure reflection, proportional to the square of the symmetry breaking order parameter, and of the **b** cell parameter, which follows the evolution of totally symmetric change (Figure 1 in [8]). Notice that a quasi-symmetrical pre-transitional evolution of this cell parameter is observed around T_{NI} , i.e., involving both sides. This is fundamentally different from most phase transitions where the pre-transitional effect only concerns the low-symmetry phase. Indeed, for a usual symmetry breaking situation (Appendix A), a linear-quadratic coupling exists between the volume strain $\varepsilon = \Delta V/V$ and the order parameter η , so proportional to $\varepsilon\eta^2$. It leads to an induced volume strain only in the low-symmetry phase that is proportional to η^2 . The observation in TTF-CA demonstrates that the bilinear coupling between the strain and the totally symmetric order parameter [41,42], proportional to $\varepsilon(q - q_c)$, is essential, underlying the importance to consider the two kinds of order parameters for a proper description of the N-I transition. However, the jump of this cell parameter at the first-order phase transition is more difficult to detect when pressure increases than the jump in the superstructure

intensity. A neutron diffraction experiment performed at higher pressure [99], and using oil as pressure transmitting medium (oblique path in the (P,T) plane), gives direct evidence of two successive anomalies in the evolution of **b** parameter with increasing temperature: the first one concomitant with the disappearance of superstructure Bragg Peaks and the second one, at higher temperature, concomitant with a change of slope in the evolution of the **a** lattice parameter. Therefore, it is reasonable to consider that, for these high pressures, the para-ferroelectric phase transition becomes separated of a totally symmetric change implying the electronic and structural state of DA chains, and which takes place at higher temperature.

This intriguing behavior is even more evident if we consider NQR studies under pressure. One should remember that this local probe is sensitive to both the symmetry breaking and the totally symmetric change. Figure 2 in [8] presents the temperature evolution at 500 MPa and 685 MPa, while the pressure evolution at 177 K is presented in Figure 11. The difference of behavior with the one at atmospheric pressure (Figure 4) is obvious. When pressure increases, there is a clear tendency toward a continuous evolution around the transition of the NQR frequencies (average one in case of I doublet) which probes the totally symmetry change. On the contrary, the ferroelectric ordering, which is probed by the splitting due to the local loss of inversion center, always presents a discontinuity at the transition. When the pressure is sufficiently high, the main part of this (average) frequency evolution occurs for temperature above the one where the splitting jumps to zero. This is shown in Figure 12 through the temperature evolution for the high-frequency NQR line of the (average) frequency and the splitting as a function of temperature at two constant pressures. On the one hand, one can still observe, both at 500 MPa and at 685 MPa, a large jump of the splitting around respectively 201 K and 240 K. This phase transition, where the ferroelectric symmetry breaking occurs, remains clearly first-order. On the other hand, at 500 MPa a discontinuity in the evolution of the (average) frequency occurs at the same temperature 201 K, while at 685 MPa the main transitional part of the evolution of the frequency, superimposed to the standard thermal evolution, is observed above 240 K. Thus, the middle frequency of the transitional part is located at about 250 K. Two discontinuities occur successively at 240 K and 250 K, but their amplitude is difficult to determine precisely. Therefore, similarly to the neutron diffraction observation, the totally symmetric change takes place at higher temperature than the ferroelectric ordering beyond some pressure.

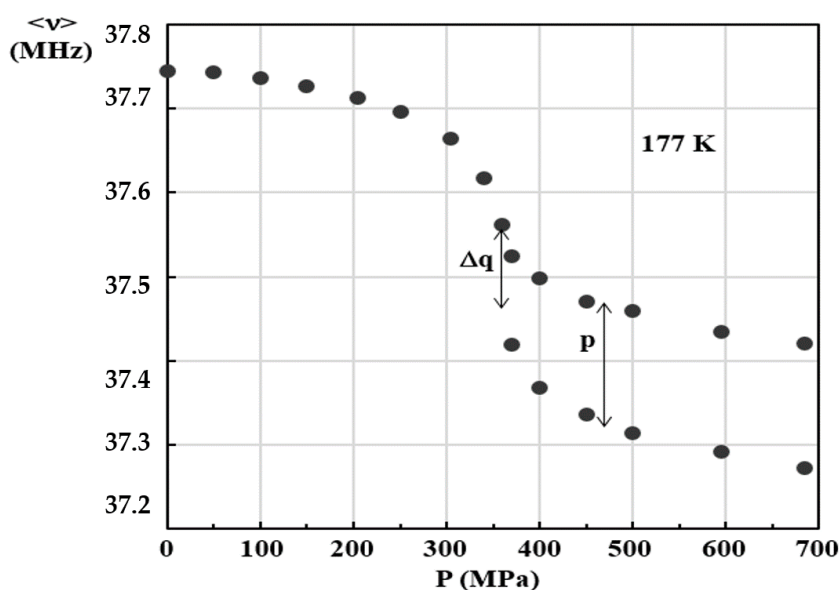


Figure 11. Pressure evolution of high-frequency chlorine Nuclear Quadrupolar Resonance (NQR) lines at 177 K.

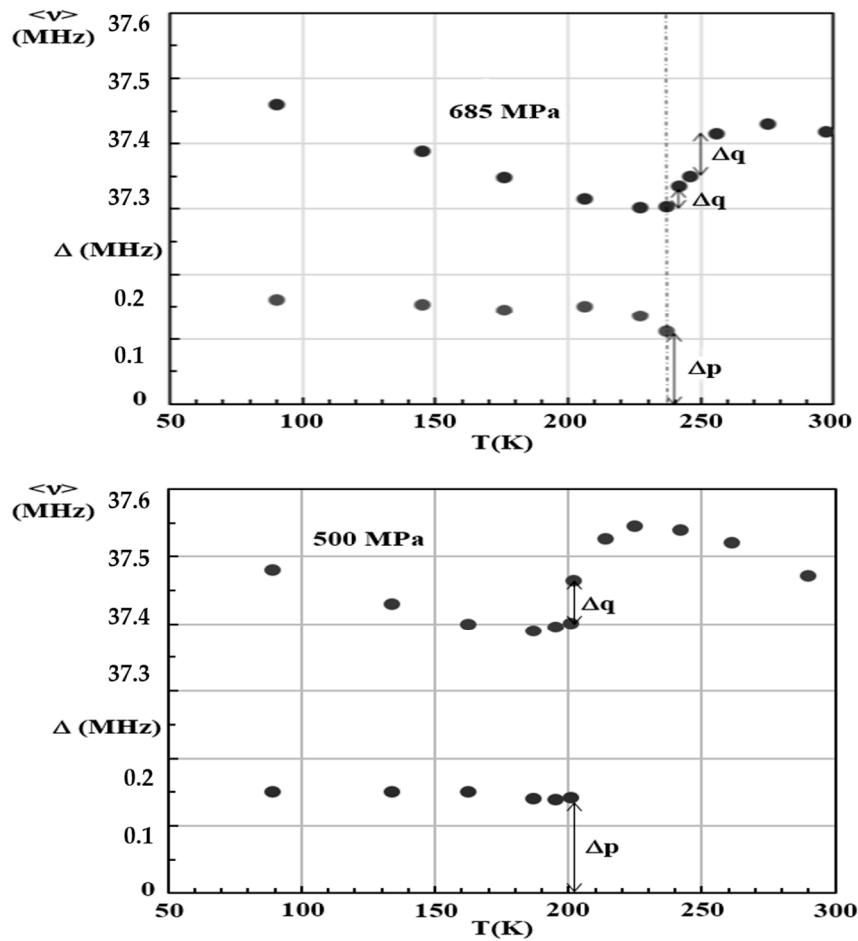


Figure 12. Temperature evolution of the (average) frequency and splitting for the high frequency NQR line at 500 MPa (bottom) and at 685 MPa (top). Adapted with permission from Reference [8]. Copyright 1997 American Physical Society.

Additional features have been obtained from dielectric measurements under pressure. Complex permittivity studies were performed in a frequency range from 1 kHz to 13 MHz in a temperature range from 80 to 300 K and under pressure up to 1 GPa, which allows to complete the phase diagram toward higher pressure. Helium was always the pressure-transmitting medium, but here the pressure losses are not compensated, yielding a pressure variation when the temperature changes (Figure 13). Previous measurements [100] have reported an anomalous dielectric response for an electric field parallel to the stacking axis **a**. A remarkable increase of the dielectric response has been observed with decreasing temperature in the N phase at ambient pressure. The results were interpreted in terms of the dynamics of NI domain walls. However, due to significant conductivity effects, the interpretation remains difficult, even more when pressure increases at room temperature. This is why our dielectric permittivity measurements are presented in Figure 13 at high frequency (13 MHz) in order to reduce the low-frequency conductivity effects. We can already observe the effect of a measurement at high frequency when we compare our results at low pressure with the previous ones performed at lower frequency. As in [100], the dielectric response in the paraelectric state is much larger, by a factor of about 30–40, for electric field directed along the stack rather than for a perpendicular direction. The response strongly increases with increasing pressure. For lower pressure a divergence-like increase is observed when cooling down to the ferroelectric transition, with a clear first-order jump of dielectric permittivity at the transition. Above about 500 MPa, this divergent-like behavior is substituted on the paraelectric side by a maximum which moves away from the ferroelectric transition (jump), and

more and more with increasing pressure. The position of this maximum is not frequency dependent, implying that it is not associated with relaxor-like behavior. The ferroelectric phase transition and the permittivity maximum are well located in the continuity of the two anomalies observed by neutron diffraction and NQR measurements, completing the phase diagram toward higher pressure.

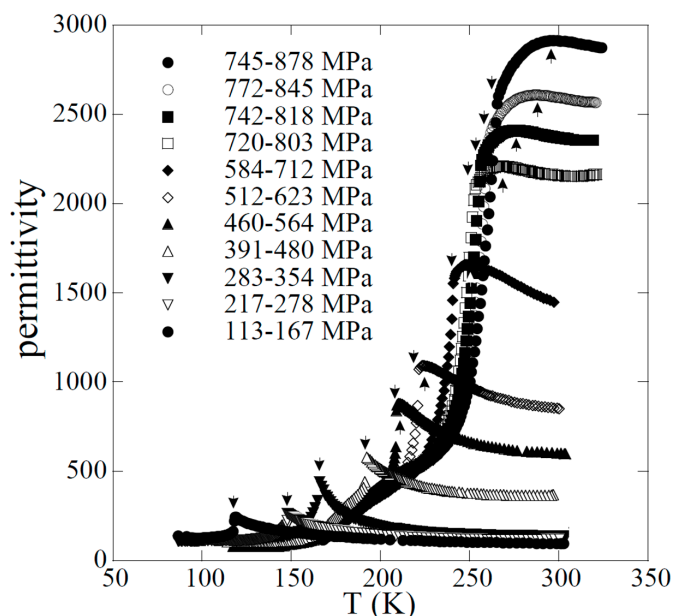


Figure 13. Temperature dependence of the dielectric permittivity measured at 13 MHz in the direction parallel to the stacking axis for different pressures. The down arrows mark the ferroelectric transition (jump) and the up arrows mark the maximum.

The consistence between the results obtained by the three experimental methods addressing different structural and electronic features is remarkable. It is clear that at sufficient pressure a totally symmetric anomaly takes place at temperature above the ferroelectric transition. Electric conductivity at room temperature, which increases remarkably by several orders of magnitude with increasing pressure, exhibits a maximum at about 870 MPa [101], quite in the prolongation of the line representing the totally symmetry anomaly. In the same way, the variation with pressure, at room temperature, of the lattice parameters exhibits a smooth anomalous evolution starting near 650 MPa and continuing until 1.1 GPa [27], i.e., surrounding the totally symmetric change up to the ferroelectric transition. Furthermore, different kinds of optical measurements under pressure, in the infrared and visible range, show a gradual evolution of spectra [102–108]. Many of them reports the coexistence of N and I molecular states and some fingerprints of local dimerization outside of the ferroelectric phase. The infrared spectra probe less directly and less precisely the evolution of the two order parameters q and p than NQR. Some intrinsic difficulties also exit in the used pressure methods to control the applied pressure. It may explain some discrepancies. In particular, a recent infrared study [108] considers a single phase transition line without the coexistence of molecular states with different ionicities. However, it is indicated that the I state appears at about 850 MPa at room temperature, which actually corresponds to the location of the totally symmetric line.

We argue that there are sufficient consistent observations to support a phase diagram quite analogous with the solid-liquid-phase transition, i.e., exhibiting when cooling above the triple point T successive totally symmetric (condensation of I pairs) and symmetry breaking (crystallization of dimerized I pairs) transition (Figure 14). Below the triple point, the two transformations take place simultaneously. Given the experimental results, we tentatively estimate the triple point to be located around 210 K and 510 MPa. The ferroelectric phase transition associated to the long range 3D polar ordering remains strongly first-order above this triple point. The discontinuity in the symmetry

breaking order parameter p is evidenced by the evolution of the superstructure intensity and NQR splitting, in agreement with the jump in permittivity. However, the first-order character is reduced more and more under pressure. This presages the existence of a tricritical point TC (relatively far from the triple point) along the ferroelectric transition line, and above which the transition becomes second-order (cf. definition of a tricritical point in Appendix A). The isostructural phase transition between two paraelectric N and I phases is characterized by a jump of the order parameter q , i.e., of the quantum or statistical average of every physical quantities involved by the totally symmetric change, including the volume as for the conventional Mott transition, and without 3D polar ordering ($p = 0$). The first-order phase transition line ends at a critical point C. Its position is difficult to determine precisely but it might be below room temperature, since the dielectric anomaly around the maximum more and more spreads out above 700 MPa. Above the critical point, this is no more a phase transition but a supercritical regime corresponding to a crossover with a smoothly evolution of the totally symmetric order parameter q and characterized by a maximum of charge fluctuations in $q_c = 1/2$ since they are proportional to $q(1 - q)$.

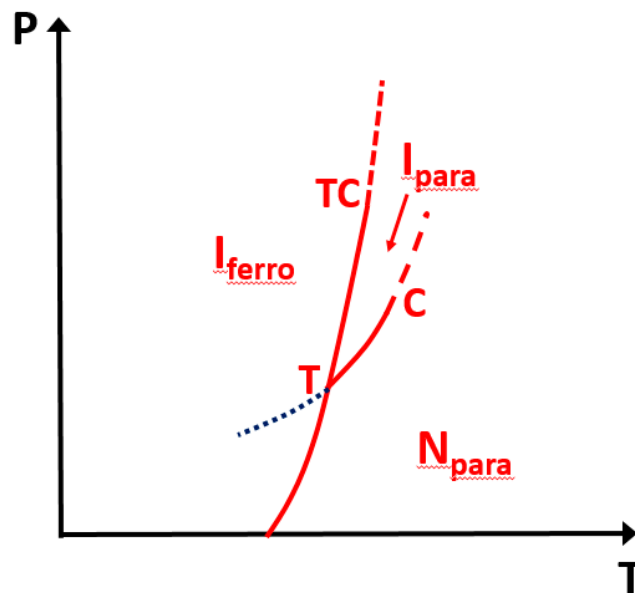


Figure 14. Schematic picture of the situation of TTF-CA through its phase diagram. Above the triple point (T), two first-order transition lines emerge: the ferro-paraelectric transition one which becomes a second-order transition line above the tricritical point (TC) and the $I_{\text{para}}-N_{\text{para}}$ isostructural one which ends at the critical point C. Above C the dotted line represents the locus of $q = q_c$ in the crossover regime (supercritical). The blue dotted line represents the hypothetic continuation of the isostructural line in the ferroelectric state.

Crossing the N-I borderline, defined by $q = q_c$, without the long range ferroelectric ordering is quite similar to the classical situation of metal-insulator Mott transition, but here it corresponds to a transition from band insulator to Mott insulator. It introduces a new Mott physics spectacularly manifested by the observation of the maximum in the dielectric permittivity (Figure 13). Within the universal frame of Landau theory, we can retrieve this behavior by using the fluctuation-response relation. Indeed, the dielectric susceptibility $\chi_p = \partial p / \partial E$ is directly related to the polarization fluctuations, i.e., only $\langle p^2 \rangle$ in the paraelectric phase. It is itself proportional to the inverse of the second partial derivative of the thermodynamic potential with respect to p (i.e., the curvature), as expressed in Equation (7):

$$\langle p^2 \rangle = k_B T \chi_p = \frac{k_B T}{\left(\frac{\partial^2 \Phi}{\partial p^2} \right)} \quad (7)$$

From the Landau potential expression (3) and only taking into account as coupling term $1/2\mu q(1 - q)p^2$, relevant near q_c , we find: $\chi \cong [A + \mu q(1 - q)]^{-1}$. Since $\mu < 0$ and $A > 0$ (paraelectric state), the susceptibility presents a maximum in $q_c = 1/2$, where the charge fluctuations are maximum. Moreover, in a quantum approach of the ground state or a one-dimensional Peierls-Hubbard model, the dielectric response peaks at the N-I transition [80]. At the concerned temperatures, the thermal charge transfer fluctuations have to be considered. As explained above, many optical measurements have reported the coexistence of N and I molecular states in the spectra, and also some signatures of local dimerization on approaching the NI borderline. These features may be interpreted within the domain-wall picture governing the dynamics of charge transfer fluctuations. The two most recent infrared studies, as a function of pressure at room temperature have been performed more accurately on a single crystal. The observed polarized absorption spectra are very similar, but the interpretation differs on several points. In the first study [105], the results are interpreted in terms of an exchange-narrowing model based on domain wall motions, when pressure crosses the NI isostructural line. When the characteristic time scale of fluctuations becomes comparable to the inverse of the difference of frequency between N and I molecular states, only a band is observed reflecting the time-averaged q , as for NQR lines in the paraelectric state. By contrast, the intramolecular N and I bands in the visible optical spectra remain well identified due to a much larger energy splitting. The typical time scale is in the picosecond (ps) range around the NI line and becomes larger of several orders of magnitude at low pressures. In the second study [106], the existence of an intermediate regime is reported, where two different I species coexist. The bandwidth of identified typical vibrational band peaks at 860 MPa, while the concentration of the I species with high ionicity increases up to 1 at 1240 MPa. Both pressures lie in the prolongation of the two branches of the phase diagram, respectively the isostructural N-I line for the lower one and the ferroelectric phase transition for the higher one.

The pressure effects in TTF-CA observed on many other physical properties can be spectacular due to the possibility of crossing the N-I line, whether it is below (first-order phase transition) or above (crossover) the critical point. As already indicated, at room temperature the electric conductivity along the stacking axis a exhibits a maximum on the N-I line [101]. To illustrate its remarkable increase from atmospheric pressure (N state) to the one where the N-I line is crossed, a recent study using accurate conductivity measurements, by employing the four-terminal method, evidences an increase of σ_{dc} from 10^{-4} to 10 S cm $^{-1}$ [109], this last one being particularly high. Moreover, the consistency between the pressure dependence of the exchange rate extracted from the exchange-narrowing model mentioned above and that of electric conductivity is impressive [106]. It illustrates that the anomalous increase of σ_{dc} may be attributed to the enhancement of the concentration and mobility of the domain wall between fluctuating N and I parts along the stacks. For a stack essentially ionic, in the ferroelectric phase or just above, the relevant excitations become charge and spin solitons [110,111]. Soliton-like paramagnetic defects have been detected by electron spin resonance [112]. At atmospheric pressure, the proton spin-lattice relaxation in the ferroelectric phase confirms the one-dimensional motion of paramagnetic centers [113,114]. A strong enhancement of their concentration under pressure is therefore expected.

4. Concluding Remarks and Perspectives

4.1. Lessons from Main Structural and Dynamical Features

The N-I transition remains a “modern old” topic where an exceptional richness of intriguing emergent phenomena driven by correlated behavior of different structural and electronic degrees of freedom has been established, while still leaving a number of essential puzzling questions. The different points can be summarized as follows:

- The analogy between the TTF-CA phase diagram and the gas-liquid-solid one is particularly illustrative of the interplay between the charge transfer instability and the ferroelectric ordering. This places the N-I transition in an exceptional situation in the universal field of phase transitions

as it combines on an equal footing isostructural transformation and symmetry breaking. On the one hand, it gives the possibility to investigate a new kind of isostructural Mott transition beyond the conventional insulator-metal Mott transition. This drives new emergent properties which remain poorly explored. The behavior under pressure is particularly exciting when the charge transfer changes smoothly above a critical point. On the other hand, the ferroelectric ordering differs on many points from usual mechanism in conventional ferroelectrics due to its strong coupling to the charge transfer instability. The NI systems occupy a unique place in the emerging field of organic ferroelectricity [115–118].

- The Landau approach, based on two strong scientific foundations, symmetry and thermodynamics, provides a universal frame to describe the N-I transition, which is unambiguous with respect to the usual reference to vaguely defined quantities such as ionicity and dimerization. The extended concept of order parameter to an isostructural situation is particularly useful. It allows to define a 2D order parameter space, involving both the (anti)ferroelectric symmetry breaking one and the totally symmetric one. This review also underlines the fact that, hidden in the order parameter description, many electronic and structural changes are involved. We stress that they may be decomposed between a part associated to the symmetry breaking and another part totally symmetric. Some Landau expansion, based on the coupling between two coupled order parameters, has been proposed and must be further explored.
- The phase transitions really take place at 3D. Therefore, the role of cooperative inter-stack interactions is essential to drive a new long range order resulting from both (anti)ferroelectric ordering and isostructural charge transfer instability. The large difference in the nature of phase transition between charge transfer crystals, with different structural array, is a good illustration of the role of inter-stack interactions. The electronic charge distribution in the unit cell is complex, but it is clear that it amplifies the inter-stack electrostatic interactions with respect to point charge models to give a significant contribution to the Madelung energy, but also to a polarization energy gain. Moreover, in connection with the volume jump at the N-I transition, occurring essentially from contraction along directions perpendicular to the stacking axis, it is also important to better explore the role of elastic inter-stack interactions, in particular their coupling with the two order parameters.
- Despite the essential role of 3D interactions in the thermodynamics of N-I phase transitions, strongly 1D dynamical fluctuations arise along the stacks in the N phase. This 1D feature is even more striking than in the well-known examples of so-called 1D molecular conductors. Therefore, we can consider these charge transfer crystalline systems as a set of 1D fluctuating objects cooperatively coupled at 3D. This is somehow an extension of the spin crossover situation where the coupled objects are actually 0D (molecule). The NI situation is obviously more complex. The 1D character enhances the electron-phonon effects along a charge transfer stack, which manifests in two limit physical pictures, the Peierls soft mode and the unconventional domain wall excitation. The debate is still open between these two limit physical pictures. If some consensus on the role of domain wall dynamics in the properties under pressure, this is not the case at ambient pressure. An intermediate situation may be also considered, with a complex spectral response combining the incomplete softening of the polar mode with a diverging slowing down of a central relaxation-type response. The energy analysis of the diffuse scattering would be important to clarify the situation.
- The high degree of covalency along stacks causes these charge transfer chains highly electrically susceptible and so drives spectacular properties. In particular, the NI system may be considered as a paradigm of electronic ferroelectricity. The N phase is a band insulator (nonmagnetic) and the I phase a Mott insulator (magnetic) and this introduces a new situation in Mott physics. It manifests by the change of sign of the dynamical effective charge at the NI transition, i.e., the anion transports a positive dynamical charge, and cation a negative. This was spectacularly evidenced in the ferroelectric phase. In addition, we report the observation of a maximum in

the dielectric response of the paraelectric state when the NI borderline is crossed. At sufficient temperature, the thermal activation of fluctuating NI domain walls becomes significant. The subsequent thermal charge fluctuations are, as the quantum one, maximum at q_c . The interplay between quantum and thermal dynamics is still poorly understood. The situation is particularly complex but opens new opportunities to understand the emergent physical properties originating from the dynamics of these unconventional excitations in 1D electron-lattice-spin systems [119], including topological solitons in I state, in particular when quantum phenomena emerge near a ferroelectric critical point [120].

4.2. New Light from Ultrafast Photo-Induced Phenomena

A very remarkable feature concerns the light or electric field pulse control of these transformations and their observation on ultra-short time scale. Another review paper of this issue on N-I transitions discusses this aspect [121]. We will simply highlight some points in connection with above discussions on electronic and structural properties. The results obtained from ultrafast experiments open new light on the N-I transition, in agreement with the adage “new eyes give rise to new ideas”. The story began with the observation at the beginning of 90’s of the laser-pulse-induced N-I transformation [12]. After this pioneering work, the field of photo-induced transitions [122,123] expanded rapidly on many and diverse directions, from correlated electrons to molecular switching, but the N-I transition remains one of the most intriguing example. On the one hand, development of ultrafast pump-probe techniques typically operating on few femtosecond (fs) time resolution, i.e., shorter than the time scale of atomic motions and molecular or material reorganization, provides an exceptional possibility to capture a real time picture of the transformation of matter. They cover diverse spectral ranges, from THz to hard X-rays. On the other hand, the number of photons per laser pulse can approach the number of photo-active species under the laser beam, and can so to prepare the material in a highly electronically excited state, affecting a macroscopic number of electrons and atoms (molecules). This very strong perturbation, producing a true “impact”, is able to drive the system in another macroscopic phase [124]. Contrary to phase transition at thermal equilibrium controlled by temperature, pressure or (static) field, the light pulse control is by nature a non-equilibrium process, even often far away from equilibrium. Another kind of non-equilibrium instability has been reported in TTF-CA through the observation of the switching between a low-conductivity state and a high-conductivity one under the controlled of a dc electric voltage [125]. It is fundamentally different from laser-pulse stimulation, since it concerns a non-equilibrium phase transition between two steady states on completely different time scales. However, it would be interesting to investigate deeper the interrelation between these two non-equilibrium and non-linear phenomena.

The possibility to trigger coherently these photo-induced phase transformations in a crystal makes the process very selective, involving only one or a few degrees of freedom, for instance one or a few phonon modes around zone center ($k = 0$), contrary to incoherent thermal excitations. It opens the possibility to “select” one or a few degrees of freedom inside the Hamiltonian. Moreover, the dynamical picture of such transformation, launched by the initial electronic excited state prepared by the fs laser pulse, is intrinsically multi-scale. The complex pathway reveals steps in time domain, since different kinds of degrees of freedom (electrons, optical and acoustical phonons) play their part on significantly different time and length scales. The ultrafast technics allow to decouple in time the different degrees of freedom, in order words to “dissect” the Hamiltonian. In contrast to thermal equilibrium phenomena, the different electronic and structural changes, involved in the order parameter description, may occur successively. The description on one scale uses information from other scale, which is typical in multi-scale phenomena. During the dynamics of given degrees of freedom, the slower ones are considered as frozen, while the faster ones act by their quantum or statistical average. It leads to bottlenecks in the state space, and there is not a unique potential picture valid at every time scales. In addition, cooperative interactions between constituents may give rise to a positive feedback of the medium, manifested by a non-linear responsiveness and threshold phenomena at some relevant stage

after the pulse. Thus, the simultaneous absorption of a huge number of photons induces more than would be the sum of individual events. More recently, high-power terahertz (THz) sources became able to engineer the state of matter through a resonant and non-resonant control [126,127]. Contrary to a visible laser pulse, a THz pulse acts on the electronic ground state, avoiding the thermal dissipation of a large part of the deposited energy in an excited electronic state. The resonant process with polar phonon modes around $k = 0$ is also very selective, triggering a large amplitude for only one or few modes (quasi-macroscopic number of phonon quanta). In addition, the amplitude of the electric field in a pulse may be around 1 MV/cm and so directly acts on the motion of electrons.

We will only comment three important features:

- The transient I-to-N transformation has been demonstrated to present some remarkable behavior on short time scale, evidenced through numerous pump-probe investigations in the visible or near-infrared spectral range [128–135], and also by time-resolved vibrational spectroscopy [136,137]. Thus, non-linear response have been observed, since at 2 ps the number of transformed DA pairs from I to N is found proportional to the number of absorbed photons, while at 500 ps it decays below a threshold value, and in contrary self-multiplies above inducing a macroscopic transformation [130,132]. In addition, in the initial linear regime the number of pairs is more than one per photon, rather estimated in the range of tens. This is explained by the induced generation of a local self-trapped N nanodomain along a stack during a first step after the absorption of one photon, in agreement with the domain-wall picture. Furthermore, the intensity of the second harmonic generation, which characterizes the ferroelectric order, decreases more rapidly and disappears before the change of reflectivity characteristic of the establishment of the N state [99]. In other words, the ferroelectric long range order is destroyed by moving NI domain-walls and also soliton-antisoliton pairs along stacks, before the isostructural transformation toward the N phase. This physical picture of a melting of the ordered structure preceding the disappearance of I species is consistent with the previous discussions on the phase diagram and it constitutes the dynamic counterpart of the static behavior.
- Many dynamical structural information can be directly probed by time-resolved X-ray or electron scattering experiments. Different X-ray diffraction and diffuse scattering investigations have been performed in TTF-CA [138–143]. One key feature is the observation of a large evolution of the intensity of some Bragg peaks in the range of 500 ps time scale after a 800 nm laser pulse irradiation of the N phase both at ESRF [138,139] and at Photon Factory [141]. In addition, some threshold effect seems to occur, but this is not again definitively established. Since the penetration depth at this wavelength is estimated to be about 2.8 μm [128], the process takes place on the slow acoustic time scale defined by the ratio between this length and the speed of sound. The recent observation of elastically driven cooperative response in a spin-crossover system is instructive [144]. It will be important to explore this point and to particularly the role of cooperative inter-stack elastic interactions. With the advent of X-ray free electron lasers new opportunities will be gained to understand the interrelation between nano-scale switching at ultra-short time scale and these process on longer spatial and temporal scales.
- Coherent oscillations were also observed in the ultrafast optical reflectivity measurements mentioned above. Thanks to a time resolution pushed down to about 20 fs, both a low-frequency lattice mode and different intra-molecular vibrations are generated after the light pulse irradiation of the N phase [135]. This shows that, as at thermal equilibrium, the photo-induced state is stabilized by triggering some deformations of the soft D and A molecules. The frequency of the lattice mode is observed in the range 53–55 cm^{-1} both above and below T_{NI} [130,132–135]. It was attributed to the dimerization intermolecular vibrations. This mode being polar this observation in N phase is *a-priori* surprising since the reflectivity is sensitive. However, we can argue that the self-trapping of I nanodomains, during the dimerization process, may generate a local symmetry breaking, which opens a channel to probe the induced electronic change of molecular state. The most surprising feature remains that the generated lattice mode keeps the same frequency in each

state and is temperature-independent, even if this dynamic picture takes place on the potential energy surface of the electronically excited state. Moreover, some new features have been recently reported with the response of the ground state of the N phase to a strong THz electric-field pulse [90]. Large induced macroscopic polarization is observed thanks to a second harmonic generation probe, with an oscillatory part. Near T_{NI} , the oscillation frequency is just below 20 cm^{-1} , which becomes close to the one reported in the infrared study at thermal equilibrium [96], and it increases with temperature increasing. The result was interpreted in terms of domain-wall dynamics, and not in terms of the B_u polar soft mode. In addition, another coherent oscillation, with a frequency of 54 cm^{-1} , is observed by probing the optical reflectivity. All these oscillatory features are very rich but remain intriguing. As at thermal equilibrium, the situation is probably complex and requires us to go beyond the limit cases of dynamical pictures.

Anyway, all these exceptional new ultrafast tools to see electrons and atoms in action shine new light on the NI physics, and many aspects remain unexplored for a large part. Thus, the new capabilities of free electron lasers have to be used. It will be crucial also to perform experiments which span a large range in spatial and temporal scales in order to investigate the intrinsic multi-scale nature of the complete transformation path, from the molecular to material scale, and from coherent dynamics, from the generation of optical phonons and propagative strain wave, to thermal stochastic phenomena, such as electron-lattice and phonon-phonon energy dissipation, heat diffusion, and so on [145]. The investigation of the kinetics to recover thermal equilibrium state, after a strong light-induced perturbation, may also provide some information on the dynamical transformation mechanism, in relation with the domain-wall dynamics [146,147]. Ultrafast high field physics is really a new adventure for the physics of correlated systems, and this is the beginning for NI systems, as for instance the observation of the modulation of ferroelectric polarization in TTF-CA [148,149] or the use of very intense electric field in ultra-short mid-infrared pulse [150]. Finally, new ideas and concepts are required and the link with theoretical approach of photo-induced phase transitions [151,152], also particularly in the N-I situation [153–158], is fundamental.

Acknowledgments: The authors want to gratefully thank S. Koshihara, M. H. Lemée-Cailleau, T. Luty and F. Moussa for their helpful contributions during our long common adventure on the structural and dynamical investigations of neutral-ionic transitions.

Author Contributions: All authors contributed equally to this work.

Conflicts of Interest: The authors declare no conflict of interest.

Appendix A. Phenomenological Landau Theory

A phase is a homogeneous macroscopic part of matter characterized by some specific electronic, magnetic and/or structural organization. A phase transition manifests by the emergence of a new long range order, and then to new macroscopic physical properties. The key feature of phase transitions at thermal equilibrium is that, despite their apparent dissimilarities illustrated by a large diversity of systems of different nature, interactions and properties, a universal description has been established: order parameter, critical phenomena . . . The Landau theory, despite of some limitations, offers a particularly universal frame to simply describe the phenomenology of phase transitions, independently of microscopic details. It is founded on two basic concepts: the order parameter and the Landau potential energy picture.

The first strong foundation of Landau theory is symmetry. Indeed, a phase transition often spontaneously manifests by a lowering of symmetry between a high-symmetry phase and a low-symmetry phase with a group-subgroup relationship. It is a symmetry breaking, since the symmetry in the low-symmetry phase has been spontaneously broken with respect to the intrinsic symmetry of the system. The symmetry breaking directly related to the occurrence of emergent properties, such as the appearance of a spontaneous electric polarization in the absence of an external electric field. The concept of order parameter has been introduced to describe the nature of symmetry

breaking, and so to characterize the new long range emergent order. The fingerprint of long range order in matter is implicitly inscribed in the relevant density function $\rho(r)$: electronic, magnetic, structural ... Actually, a long range order in the crystalline state is described by a density function which is the periodic repetition of $\rho_{\text{cell}}(r)$, the average over all unit cells. Within the frame of Landau theory, it can be decomposed as in Equation (A1):

$$\rho(r) = \rho_0(r) + \Delta\rho(r) \quad (\text{A1})$$

where ρ_0 is left invariant by the elements of the initial symmetry group G_0 of the high-symmetry phase and $\Delta\rho$ is the change of density function to form the low-symmetry phase, described by a symmetry group G subgroup of G_0 . The method of analyzing symmetry variation is based on expanding $\Delta\rho$ in terms of an irreducible representation (IR) of G_0 , as shown in Equation (A2):

$$\Delta\rho(r) = \sum_i \eta_i \phi_i(r) \quad (\text{A2})$$

where the η_i are the vector component of the order parameter η of dimension equal to that of the IR and the $\phi_i(r)$ the basis function of the same IR [159]. The order parameter η describes in which way the low-symmetry phase deviates from the initial high-symmetry. Its modulus, which is only non-zero in the unsymmetrical phase, measures the degree of symmetry breaking. The spontaneous order parameter can become very small when it goes to zero continuously on approaching a critical temperature, i.e., in case of a second order phase transition. On the contrary, it presents a jump to zero at the transition temperature for a first-order phase transition.

In crystalline state one has to consider the representations of crystal space groups. The translational symmetry of the function ϕ_i , is described by a given wave vector \mathbf{k}_0 which determines the new periodicity of the lattice in the low-symmetry phase. The situation is particularly simple in the case of a symmetry breaking without change of cell multiplicity. This is characterized by $\mathbf{k}_0 = 0$ (zone-center) and the relevant IR are those of the point group. For the sake of illustration, we will consider the concrete problem of the change of symmetry $2/m \rightarrow m$. The crystal loses the inversion center (polar group) and the two-fold axis, but keeps the plane of symmetry. The IR of $2/m$ are one-dimensional and the order parameter has one-component (scalar) of B_u symmetry. There are only two equivalent macroscopic states $+\eta$ and $-\eta$ which corresponds to the formation of two kinds of macroscopic domains, i.e., the crystals may be divided into regions which differs by the sign of the order parameter η . In this example with polar order, it corresponds to ferroelectric domains with reverse polarizations.

The second strong foundation is the thermodynamics. A great advantage of the Landau description is to use a simple potential energy picture, which is the simplest way to discuss the stability, metastability and instability of a system. It is based on the grounds of the Landau expansion of the relevant thermodynamic potential Φ , such as free energy, as a function of the order parameter η for given values of control parameters, temperature, pressure, electric or magnetic field ... The polynomial terms should be invariant under all symmetry operations of the group G_0 . In the simple example discussed above, the order parameter is scalar and therefore the Landau potential which determines the spontaneous ordering in zero external field has to respect the symmetry $\Phi(\eta) = \Phi(-\eta)$ and so it contains only even terms (Equation (A3)):

$$\Phi(\eta) = \Phi_0 + \frac{1}{2}A\eta^2 + \frac{1}{4}B\eta^4 + \frac{1}{6}C\eta^6 + \dots \quad (\text{A3})$$

Φ_0 , A , B and C are depending of the control thermodynamic parameters T and P . The extrema of this potential energy function determines the equilibrium states. The sign of the phenomenological coefficient A determines if the state $\eta = 0$ is (meta)stable ($A > 0$) or unstable ($A < 0$). For $B > 0$, a second order phase transition takes place at $A = 0$, between the high-symmetry phase (for $A > 0$ single-well

potential with a minimum at $\eta = 0$) and the low-symmetry one (for $A < 0$ symmetrical double-well potential). The relation $A(P,T) = 0$ defines a second order phase transition line, i.e., the locus of critical points. The simplest way to describe the temperature evolution of Φ around the critical temperature T_c at a given pressure P is to consider a linear dependence (Equation (A4)):

$$A(T) = a(T - T_c), \quad (\text{A4})$$

with generally $a > 0$. The equilibrium states results from the equilibrium condition $\partial\Phi/\partial\eta = 0$. Below T_c the two stable states for the order parameter are such as $\eta_0^2 \approx (T - T_c)$. We can also take into account the effect of a field H conjugate to the order parameter η by the addition of a coupling term $-H\eta$. The application of a field breaks the symmetry and then $H > 0$ favors the state $+\eta$. In the (H,T) phase diagram an horizontal first-order phase transition line, defined by $H = 0$, ends to a critical point at T_c . When crossing vertically the transition line below T_c , the order parameter switches from $+(-)$ to $-(+)$ η_0 . A bistable regime occurs inside some metastability limits, the two so-called spinodal lines, which gives rise to a field hysteresis phenomena, such as ferroelectric hysteresis. It can be obtained from the equation of state $H \cong 2A\eta + 4B\eta^3$. This cubic equation has only one solution for $A > 0$ ($T > T_c$), and up to three (real) solutions for $A < 0$ ($T < T_c$), respectively corresponding to a stable state, a metastable and an unstable between the two other ones. The curve $\eta(H)$ resulting from the equation of state become S-shaped. Moreover, in the case $B < 0$, the transition becomes first-order with a jump in the temperature evolution of the order parameter at the transition temperature T_0 . This results from the occurrence of a symmetrical triple-well potential with three minima to 0, $+\eta_0$ and $-\eta_0$ which become energetically equivalent at $T_0 > T_c$ (assuming $C > 0$). This is another kind of multistable regime which gives rise to thermal hysteresis. In a (T,P) phase diagram T a line of second-order phase transition (critical points) establishes in the region where $B(T,P) > 0$, before crossing the line $B(P,T) = 0$ at a so-called tricritical point and followed by a first-order phase transition line on the other side. A current explanation of such a first-order behaviour is discussed in terms of the coupling of order parameter with volume strain, particularly strong in structural phase transitions. In the simple example discussed above, the phase transition is non-ferroelastic, i.e., it keeps the same crystalline system. It only implies a volume strain $\varepsilon = \Delta V/V$, which is a totally symmetric parameter. In the Landau expansion, two terms are added, the elastic energy $\frac{1}{2} K\varepsilon^2$ and a linear-quadratic coupling $\alpha\varepsilon\eta^2$ in order to respect the invariance under the transformation of the group G_0 . The condition of equilibrium for Φ with respect of the two parameters η and ε leads to two coupled equations. There are two main physical consequences: on the one hand, a coupled volume strain in the low-symmetry phase proportional to η^2 , and on the other hand, a new effective coefficient $B^* = B - 2\alpha^2/K$ which can become < 0 (first-order transition).

There also exist phase transitions without change of symmetry, such as the Mott transition or the spin transition, for examples. They are generally called isostructural phase transitions and are analogous to the gas-liquid phase transition, with a $(P-T)$ phase diagram composed of a first-order line (coexistence line) ending at a critical point. It is not possible to define an order parameter in the sense of symmetry breaking. But, it is known that the thermodynamics of the gas-liquid phase transition presents phenomenological similarities with the one of ferromagnetic systems. Actually, the discontinuity of the density ρ for a fluid along the first-order line in the thermodynamic control parameter space (P,T) plays the same role that the magnetization jump along the horizontal first-order line in the (H,T) phase diagram. This extends the concept of order parameter to a totally symmetrical (nonsymmetry breaking) order parameter η , but in this case the expansion of the thermodynamic potential Φ contains also odd term (Equation (A5)):

$$\Phi(\eta) = \Phi_0 + \alpha\eta + \frac{1}{2}\beta\eta^2 + \frac{1}{3}\gamma\eta^3 + \frac{1}{4}\delta\eta^4 + \dots \quad (\text{A5})$$

It can be shown that by a convenient change of variable $\eta \rightarrow x$ the third-order term [33] can be eliminated and therefore, up to the fourth-order term, the expression of the thermodynamic potential becomes as in Equation (A6):

$$\Phi(x) = \Phi_0 + \frac{1}{4}A'x^2 + \frac{1}{4}B' - H'x. \quad (\text{A6})$$

It indicates that, in a first approximation neglecting the higher-order odd terms, the thermodynamics which determines the potential picture for the totally symmetric order parameter x is quite similar with the one in the previous symmetry breaking situation in presence of field. Actually, this approximation amounts to the same thing as to draw in the (P-T) phase diagram an axis A' tangentially to the first order line at the critical point and an axis H' perpendicularly (Figure 5), and to define as order parameter $x = (\rho - \rho_c)$ where ρ_c is the value of the critical density at the critical end point, or for the spin transition $x = (n - n_c)$ where n is the concentration of high-spin molecules and $n_c = 1/2$ (32). However, the description around the transition of $x(T)$ at P constant, or vice-versa, implies to cross the horizontal transition line ($H' = 0$) along an oblique path. A bistable regime exists below T_c , limited by two spinodal lines. The two macroscopic equilibrium states which exist between these two spinodal lines are equally stable only on the first-order line. The metastable state disappears beyond the two spinodal lines. The thermal hysteresis which occurs when crossing the first-order transition line in the (P-T) phase diagram has actually a similar origin as the one under field for a symmetry breaking situation, with an equally S-shaped $x(H')$ curve at temperature $T < T_c$. Above the critical point, there is no more a phase transition but a crossover, as it is well established for the gas-liquid supercritical regime. One can also underline the qualitative similarities of behavior between the one obtained from the equation of state $H' = 2A'x + 4B'x^3$ and the one resulting from the van der Waals equation.

In statistical physics, the validity of this analytic Landau expansion is based on mean field approximation. This is well known in the physics critical phenomena through the Ising model or the equivalent lattice-gas model. However, the critical regime where the thermodynamic behavior is dominated by the fluctuations, i.e., when the mean field approximation fails, generally extends on a small fraction of the temperature range around the critical temperature. In low-dimensional systems, and particularly in 1D, critical fluctuations develop easily. However, the mean field approximation becomes valid in the case of long range electric or elastic interactions.

References

1. Torrance, J.B.; Vazquez, J.E.; Mayerle, J.J.; Lee, V.Y. Discovery of a neutral-to-ionic phase transition in organic materials. *Phys. Rev. Lett.* **1981**, *46*, 253–257. [[CrossRef](#)]
2. Saito, G.; Yoshida, Y. Development of conductive molecular assemblies: Organic metals, superconductors, and exotic functional materials. *Bull. Chem. Soc. Jpn.* **2007**, *80*, 1–137. [[CrossRef](#)]
3. Torrance, J.B. An overview of organics solids: The relation between their electronic, optical, magnetic and structural properties. In *Low-Dimensional Conductors and Superconductors*; Jerome, D., Ed.; Springer: New York, NY, USA, 1987; pp. 113–133.
4. Torrance, J.B.; Girlando, A.; Mayerle, J.J.; Crowley, J.I.; Lee, V.Y.; Batail, P.; LaPlaca, S.J. Anomalous nature of neutral-to-ionic phase transition in tetrathiafulvalene-chloranil. *Phys. Rev. Lett.* **1981**, *47*, 1747–1750. [[CrossRef](#)]
5. Jacobsen, C.S.; Torrance, J.B. Behavior of charge-transfer absorption upon passing through the neutral-ionic phase transition. *J. Chem. Phys.* **1983**, *79*, 1075–1085. [[CrossRef](#)]
6. Buron-Le Cointe, M.; Lemée-Cailleau, M.H.; Cailleau, H.; Toudic, B.; Moréac, A.; Moussa, M.; Ayache, C.; Karl, N. Thermal hysteresis and mesoscopic phase coexistence around the neutral-ionic phase transition in TTF-CA and TMB-TCNQ. *Phys. Rev. B* **2003**, *68*, 064103. [[CrossRef](#)]
7. Le Cointe, M.; Lemée-Cailleau, M.H.; Cailleau, H.; Toudic, B.; Toupet, L.; Heger, G.; Moussa, F.; Schweiss, P.; Kraft, K.H.; Karl, N. Symmetry breaking and structural changes at the neutral-to-ionic transition tetrathiafulvalene-*p*-chloranil. *Phys. Rev. B* **1995**, *51*, 3374–3386. [[CrossRef](#)]

8. Lemée-Cailleau, M.H.; Le Cointe, M.; Cailleau, H.; Luty, T.; Moussa, F.; Roos, J.; Brinkmann, D.; Toudic, B.; Ayache, C.; Karl, N. Thermodynamics of the neutral-to-ionic transition as condensation and crystallization of charge-transfer excitations. *Phys. Rev. Lett.* **1997**, *79*, 1690–1693. [[CrossRef](#)]
9. Kobayashi, K.; Horiuchi, S.; Kumai, R.; Kagawa, F.; Murakami, Y.; Tokura, Y. Electronic ferroelectricity in a molecular crystal with large polarization directing antiparallel to ionic displacement. *Phys. Rev. Lett.* **2012**, *108*, 237601. [[CrossRef](#)] [[PubMed](#)]
10. Collet, E.; Lemée-Cailleau, M.H.; Buron-Le Cointe, M.; Cailleau, H.; Ravy, S.; Luty, T.; Béar, J.F.; Czarnecki, P.; Karl, N. Direct evidence of lattice-relaxed charge transfer exciton strings. *Europhys. Lett.* **2002**, *57*, 67–73. [[CrossRef](#)]
11. Buron-Le Cointe, M.; Lemée-Cailleau, M.H.; Cailleau, H.; Ravy, S.; Béar, J.F.; Rouzière, S.; Elkaïm, E.; Collet, E. One-dimensional fluctuating nanodomains in the charge-transfer molecular system TTF-CA and their first-order crystallisation. *Phys. Rev. Lett.* **2006**, *96*, 205503. [[CrossRef](#)] [[PubMed](#)]
12. Koshihara, S.; Tokura, Y.; Mitani, T.; Saito, G.; Koda, T. Photoinduced valence instability in the organic molecular compound tetrathiafulvalene-*p*-chloranil (TTF-CA). *Phys. Rev. B* **1990**, *42*, 6853–6856. [[CrossRef](#)]
13. Strukov, B.A.; Levanyuk, A.P. *Ferroelectric Phenomena in Crystals: Physical Foundations*; Springer: Berlin/Heidelberg, Germany; New York, NY, USA, 1998.
14. D’Avino, G.; Painelli, A.; Soos, Z.G. Modelling the neutral-ionic transition with correlated electrons coupled to soft lattices and molecules. *Crystals* **2017**, *7*, 144. [[CrossRef](#)]
15. Oison, V.; Katan, C.; Rabiller, P.; Souhassou, M.; Koenig, C. Neutral-ionic phase transition: A thorough ab-initio study of TTF-CA. *Phys. Rev. B* **2003**, *67*, 035120. [[CrossRef](#)]
16. Delchiaro, F.; Girlando, A.; Painelli, A.; Bandyopadhyay, A.; Patti, S.K.; D’Avino, G. Towards first-principles prediction of valence instabilities in mixed stack charge-transfer crystals. *Phys. Rev. B* **2017**, *95*, 155125. [[CrossRef](#)]
17. Tokura, Y.; Koda, T.; Mitani, T.; Saito, G. Neutral-to-ionic transition in tetrathiafulvalene-*p*-chloranil as investigated by optical reflection spectra. *Solid State Commun.* **1982**, *43*, 757–760. [[CrossRef](#)]
18. Girlando, A.; Marzola, F.; Pecile, C.; Torrance, J.B. Vibrational spectroscopy of mixed stack organic semiconductors: Neutral and ionic phases of tetrathiafulvalene-chloranil (TTF-CA) charge transfer complex. *J. Chem. Phys.* **1983**, *79*, 1075–1085. [[CrossRef](#)]
19. Dressel, M.; Peterseim, T. Infrared investigations of the neutral-ionic phase transition in TTF-CA and its dynamics. *Crystals* **2017**, *7*, 17. [[CrossRef](#)]
20. Masino, M.; Castagnetti, N.; Girlando, A. Phenomenology of the neutral-ionic valence instability in mixed stack charge-transfer crystals. *Crystals* **2017**, *7*, 108. [[CrossRef](#)]
21. Katan, C. First-principles study of the structures and vibrational frequencies for tetrathiafulvalene TTF and TTF-*d*₄ in different oxidation states. *J. Phys. Chem. A* **1999**, *103*, 1407–1413. [[CrossRef](#)]
22. Resta, R. Charge states in Transition. *Nature* **2008**, *453*, 735. [[CrossRef](#)] [[PubMed](#)]
23. Garcia, P.; Dahanoui, S.; Katan, C.; Souhassou, M.; Lecomte, C. On the accurate estimation of intermolecular interactions and charge transfer: The case of TT-CA. *Faraday Discuss.* **2007**, *135*, 217–235. [[CrossRef](#)] [[PubMed](#)]
24. Gourdji, M.; Guibé, L.; Peneau, A.; Gallier, J.; Toudic, B.; Cailleau, H. Cl-35 NQR observation of the neutral-to-ionic phase-transition in tetrathiafulvalene-para-chloranil. *Solid State Commun.* **1991**, *77*, 609–612. [[CrossRef](#)]
25. Gallier, J.; Toudic, B.; Delugeard, Y.; Cailleau, H.; Gourdji, M.; Peneau, A.; Guibé, L. Chlorine-nuclear-quadrupole-resonance study of the neutral-to-ionic transition in tetrathiafulvalene-chloranil. *Phys. Rev. B* **1993**, *47*, 11688–11695. [[CrossRef](#)]
26. Le Cointe, M.; Gallier, J.; Cailleau, H.; Gourdji, M.; Peneau, A.; Guibé, L. ³⁵Cl NQR study on TTF-CA crystals: Symmetry lowering and hysteresis at the neutral-to-ionic transition. *Solid State Commun.* **1995**, *94*, 455–459. [[CrossRef](#)]
27. Metzger, R.M.; Torrance, J.B. Role of the Madelung energy at the neutral-ionic phase transition of tetrathiafulvalene chloranil. *J. Am. Chem. Soc.* **1985**, *107*, 117–121. [[CrossRef](#)]
28. Kawamoto, T.; Izuka-Sakano, T.; Shimoi, Y.; Abe, S. Crucial effects of intramolecular charge distribution on the neutral-ionic transition of tetrathiafulvalene-*p*-chloranil. *Phys. Rev. B* **2001**, *64*, 205107. [[CrossRef](#)]
29. Bartholin, H.; Baudour, J.L.; Breandon, C.; Tchaptoutian, R.; Cailleau, H.; Perrin, D. A possible devil’s staircase in TTF-chloranil at the neutral-ionic transition observed by electric conductivity measurements. *Solid State Commun.* **1987**, *63*, 223–225. [[CrossRef](#)]

30. Ayache, C.; Torrance, J.B. Multiple specific heat anomalies at the neutral-ionic phase transition in TTF-chloranil. *Solid State Commun.* **1983**, *47*, 789–793. [[CrossRef](#)]
31. Kishida, H.; Takamatsu, H.; Fujinuma, K.; Okamoto, H. Ferroelectric nature and real-space observations of domain motions in the organic charge-transfer compound tetrathiafulvalene-*p*-chloranil. *Phys. Rev. B* **2009**, *80*, 205201. [[CrossRef](#)]
32. Halcrow, M.A. *Spin-Crossover Materials: Properties and Applications*; John Wiley & Sons: Chichester, UK, 2013.
33. Kuznetsov, A.Y.; Dimitriev, V.P.; Bandilet, O.I.; Weber, H.P. High-temperature fcc phase of Pr: Negative thermal expansion and intermediate valence state. *Phys. Rev. B* **2003**, *68*, 064109. [[CrossRef](#)]
34. Avignon, M.; Balseiro, C.A.; Protteo, C.R.; Alascio, B. Neutral-ionic transition and dimerization in organic mixed-stack compounds. *Phys. Rev. B* **1986**, *33*, 205–209. [[CrossRef](#)]
35. Chernyshov, D.; Bürgi, H.B.; Hostettler, M.; Törnroos, K.W. Landau theory for spin transition and ordering phenomena in Fe(II) compounds. *Phys. Rev. B* **2004**, *70*, 094116. [[CrossRef](#)]
36. Iizuka-Sakano, T.; Toyozawa, Y. The role of long range Coulomb interaction in the neutral-to-ionic transition of quasi-one-dimensional charge transfer compounds. *J. Phys. Soc. Jpn.* **1996**, *65*, 671–674. [[CrossRef](#)]
37. Soos, Z.G.; Painelli, A. Metastable domains and potential energy surfaces in organic charge-transfer salts with neutral-ionic phase transitions. *Phys. Rev. B* **2007**, *75*, 155119. [[CrossRef](#)]
38. Yi, T.; Kirova, N.; Brazovskii, S. Dynamical patterns of phase transformations from self-trapping of quantum excitons. *Phys. B* **2015**, *460*, 73–78. [[CrossRef](#)]
39. Rushchanskii, K.Z.; Vysochanskii, Y.M.; Strauch, D. Ferroelectricity, nonlinear dynamics, and relaxation effects in monoclinic Sn₂P₂S₆. *Phys. Rev. Lett.* **2007**, *99*, 207601. [[CrossRef](#)] [[PubMed](#)]
40. Luty, T. *Neutral-to-Ionic Transformation as Condensation and Solidification of Charge-Transfer Excitations. Relaxations of Excited States and Photo-Induced Structural Phase Transitions*; Nasu, K., Ed.; Springer Series in Solid-State Sciences; Springer: Berlin/Heidelberg, Germany, 1997; Volume 124, pp. 142–150.
41. Kishine, J.; Luty, T.; Yonemitsu, K. Ferroelectric phase transition, ionicity condensation, and multicriticality in charge-transfer complexes. *Phys. Rev. B* **2004**, *69*, 075115. [[CrossRef](#)]
42. Kishine, J.; Ohara, T.; Luty, T.; Yonemitsu, K. Inter-chain Coulomb-lattice Relaxation and multicriticality in charge transfer organic complexes. *Synth. Met.* **2005**, *154*, 257–260. [[CrossRef](#)]
43. Blume, M.; Emery, V.J.; Griffiths, R.B. Ising model for the λ transition and phase separation in He³-He⁴ mixtures. *Phys. Rev. A* **1971**, *4*, 1071–1077. [[CrossRef](#)]
44. Lajzerowicz, J.; Sivardière, J. Spin-1 lattice-gas model. I. Condensation and solidification of a simple fluid. *Phys. Rev. A* **1975**, *11*, 2079–2089. [[CrossRef](#)]
45. Luty, T. Ground state phase diagram of mixed-stack compounds with intermolecular electron transfer. *Acta Phys. Pol. A* **1995**, *87*, 1009–1021. [[CrossRef](#)]
46. Otsuka, Y.; Seo, H.; Yoshimi, K.; Kato, T. Finite temperature neutral-ionic transition and lattice dimerization in charge-transfer complexes: QCM study. *Phys. B* **2012**, *407*, 1793–1795. [[CrossRef](#)]
47. Aoki, S.; Nakayama, T.; Miura, A. Temperature-induced neutral-ionic transition in dimethyltetrathiafulvalene-*p*-chloranil. *Phys. Rev. B* **1993**, *48*, 626–629. [[CrossRef](#)]
48. Collet, E.; Buron-Le Cointe, M.; Lemée-Cailleau, M.H.; Cailleau, H.; Toupet, L.; Meven, M.; Mattauch, S.; Heger, G.; Karl, N. Structural evidence of ferroelectric neutral ionic layered ordering in 2,6-dimethyltetrathiafulvalene-*p*-chloranil. *Phys. Rev. B* **2001**, *63*, 054105. [[CrossRef](#)]
49. Horiuchi, S.; Okimoto, Y.; Kumai, R.; Tokura, Y. Quantum phase transition in organic charge-transfer complexes. *Science* **2003**, *299*, 229–232. [[CrossRef](#)] [[PubMed](#)]
50. Okimoto, Y.; Kumai, R.; Horiuchi, S.; Okamoto, H.; Tokura, Y. Quantum neutral-ionic phase transition as investigated by Raman scattering and X-ray diffraction. *J. Phys. Soc. Jpn.* **2005**, *74*, 2165–2168. [[CrossRef](#)]
51. Toledano, J.C.; Toledano, P. *The Landau Theory of Phases Transitions*; World Scientific: Singapore, 1987.
52. Oison, V.; Rabiller, P.; Katan, C. Theoretical investigation of the ground state properties of DMTTF-CA: A step toward the understanding of charge transfer complexes undergoing the neutral-to-ionic phase transition. *J. Phys. Chem. A* **2004**, *108*, 11049–11055. [[CrossRef](#)]
53. Tolédano, P.; Guennou, M. Theory of antiferroelectric phase transitions. *Phys. Rev. B* **2016**, *94*, 014107. [[CrossRef](#)]
54. Iwase, F.; Miyagawa, K.; Fujiyama, S.; Kanoda, K.; Horiuchi, S.; Tokura, Y. Neutral-ionic phase transition in DMTTF-QCl₄ investigated by ³⁵Cl NQR. *J. Phys. Soc. Jpn.* **2007**, *76*, 073701. [[CrossRef](#)]

55. Bachheimer, J.P.; Dolino, G. Measurement of the order parameter of α -quartz by second-harmonic generation of light. *Phys. Rev. B* **1975**, *11*, 3195–3205. [[CrossRef](#)]
56. Ranzieri, P.; Masino, M.; Girlando, A.; Lemée-Cailleau, M.H. Temperature-induced valence and structural instability in DMTTF-CA: Single-crystal Raman and infrared measurements. *Phys. Rev. B* **2007**, *76*, 134115. [[CrossRef](#)]
57. Castagnetti, N.; Kociok-Köhn, G.; Da Como, E.; Girlando, A. Temperature-induced valence instability in the charge-transfer crystal TMB-TCNQ. *Phys. Rev. B* **2017**, *95*, 024101. [[CrossRef](#)]
58. Horiuchi, S.; Okimoto, Y.; Kumai, R.; Tokura, Y. Anomalous valence fluctuations near a ferroelectric transition in an organic charge-transfer complex. *J. Phys. Soc. Jpn.* **2000**, *69*, 1302–1305. [[CrossRef](#)]
59. Girlando, A.; Pecile, C.; Torrance, J.B. A key to understanding ionic mixed stack organic solids: Tetrathiafulvalene-bromanil. *Solid State Commun.* **1985**, *54*, 753–759. [[CrossRef](#)]
60. Garcia, P.; Dahaoui, S.; Fertey, P.; Wenger, E.; Lecomte, C. Crystallographic investigation of temperature-induced phase transition of the tetrathiafulvalene-*p*-bromanil TTF-BA charge-transfer complex. *Phys. Rev. B* **2005**, *72*, 104115. [[CrossRef](#)]
61. Kagawa, F.; Horiuchi, S.; Tokunaga, M.; Fujioka, J.; Tokura, Y. Ferroelectricity in one-dimensional organic quantum magnet. *Nat. Phys.* **2010**, *6*, 169–172. [[CrossRef](#)]
62. Horiuchi, S.; Okimoto, Y.; Kumai, R.; Tokura, Y. Ferroelectric valence transition and phase diagram of a series of charge-transfer complexes of 4,4'-dimethyltetrathiafulvalene and tetrahalo-*p*-benzoquinones. *J. Am. Chem. Soc.* **2001**, *123*, 665–670. [[CrossRef](#)] [[PubMed](#)]
63. Iwase, F.; Miyagawa, K.; Kanoda, K.; Horiuchi, S.; Tokura, Y. NQR study of neutral-ionic phase transition and quantum paraelectric state in organic charge-transfer complexes. *Solid State Sci.* **2008**, *10*, 1752–1756. [[CrossRef](#)]
64. Lemée-Cailleau, M.H.; Collet, E.; Buron-Le Cointe, M.; Grach, N.; Ouladdiaf, B.; Moussa, F.; Hasegawa, T.; Takahashi, Y.; Roisnel, T.; Cailleau, H. Down to the quantum limit at the neutral-to-ionic phase transition of (BEDT-TTF)-(ClMe-TCNQ): Symmetry analysis and phase diagram. *J. Phys. Chem. B* **2007**, *111*, 6167–6172. [[CrossRef](#)] [[PubMed](#)]
65. Miyasaka, H.; Motokawa, N.; Chiyo, T.; Takemura, M.; Yamashita, M.; Sagayama, H.; Arima, T. Stepwise neutral-ionic phase transitions in a covalently bonded donor/acceptor chain compound. *J. Am. Chem. Soc.* **2011**, *133*, 5338–5345. [[CrossRef](#)] [[PubMed](#)]
66. Ishibashi, S.; Terakura, K. First-principles study of spontaneous polarization in tetrathiafulvalene-*p*-chloranil. *Phys. B* **2010**, *405*, S338–S340. [[CrossRef](#)]
67. Giovannetti, G.; Kumar, S.; Stroppa, A.; van den Brink, J.; Picozzi, S. Multiferroelectricity in TTF-CA organic molecular crystals predicted through ab initio calculations. *Phys. Rev. Lett.* **2009**, *103*, 266401. [[CrossRef](#)] [[PubMed](#)]
68. Dawber, M. Viewpoint: Electrons weight in on Ferroelectricity. *Physics* **2012**, *5*, 63. [[CrossRef](#)]
69. King-Smith, R.D.; Vanderbilt, D. Theory of polarization of crystalline solids. *Phys. Rev. B* **1993**, *47*, 1651–1654. [[CrossRef](#)]
70. Resta, R. Macroscopic polarization as geometric quantum phase. *Europhys. Lett.* **1993**, *22*, 133–138. [[CrossRef](#)]
71. Resta, R. Macroscopic polarization in crystalline dielectrics: The geometric phase approach. *Rev. Mod. Phys.* **1994**, *66*, 899–915. [[CrossRef](#)]
72. Spaldin, N.A. A beginner's guide to the modern theory of polarization. *J. Solid State Chem.* **2012**, *195*, 2–10. [[CrossRef](#)]
73. Ishibashi, S.; Terakura, K.; Horiuchi, S. First-principles electronic structure study for organic ferroelectric tetrathiafulvalene-*p*-bromanil. *J. Phys. Soc. Jpn.* **2010**, *79*, 043703. [[CrossRef](#)]
74. Egami, T.; Ishihara, S.; Tachiki, M. Lattice effect of strong electron correlation: Implication for ferroelectricity and superconductivity. *Science* **1993**, *261*, 1307–1310. [[CrossRef](#)] [[PubMed](#)]
75. Ishihara, S.; Egami, T.; Tachiki, M. Enhancement of the electron-lattice interaction due to strong electron correlation. *Phys. Rev. B* **1994**, *49*, 8944–8954. [[CrossRef](#)]
76. Ishihara, S.; Tachiki, M.; Egami, T. Covalency contributions to the electronic polarizability in dielectric compounds. *Phys. Rev. B* **1994**, *49*, 16123–16128. [[CrossRef](#)]
77. Resta, R.; Sorella, S. Many-body effects on polarization and dynamical charges in a partly covalent polar insulator. *Phys. Rev. Lett.* **1995**, *74*, 4738–4741. [[CrossRef](#)] [[PubMed](#)]

78. Pike, N.A.; Van Troeye, B.; Dewandre, A.; Petretto, G.; Gonze, X.; Rignanese, G.M.; Verstraete, J. Origin of the counterintuitive dynamic charge in the transition metal dichalcogenides. *Phys. Rev. B* **2017**, *95*, 201106. [[CrossRef](#)]
79. Del Freo, L.; Painelli, A.; Soos, Z.G. Giant infrared intensity of the Peierls mode at the neutral-ionic phase transition. *Phys. Rev. Lett.* **2002**, *89*, 027402. [[CrossRef](#)] [[PubMed](#)]
80. Soos, Z.G.; Bewick, S.A.; Peri, A.; Painelli, A. Dielectric response of modified Hubbard models with neutral-ionic and Peierls transitions. *J. Chem. Phys.* **2004**, *120*, 6712–6720. [[CrossRef](#)] [[PubMed](#)]
81. D'Avino, G.; Verstraete, M.J. Are hydrogen-bonded charge transfer crystals room temperature ferroelectrics? *Phys. Rev. Lett.* **2014**, *113*, 237602. [[CrossRef](#)] [[PubMed](#)]
82. Ishibashi, S.; Terakura, K. Exotic ferroelectricity in tetrathiafulvalene-*p*-chloranil: Anomalous effective charges and a picture in the framework of maximally localized Wannier orbitals. *J. Phys. Soc. Jpn.* **2014**, *83*, 073702. [[CrossRef](#)]
83. Tekakura, K.; Ishibashi, S. Mechanism of covalency-induced electric polarization within the framework of maximally localized Wannier orbitals. *Phys. Rev. B* **2015**, *91*, 195120. [[CrossRef](#)]
84. Ravy, S. Study of molecular conductors by X-ray diffuse scattering. *Chem. Rev.* **2004**, *104*, 5609–5634. [[CrossRef](#)] [[PubMed](#)]
85. Nagaosa, N.; Takimoto, J. Theory of neutral-ionic transition in organic crystals. I. Monte Carlo simulation of modified Hubbard model. *J. Phys. Soc. Jpn.* **1986**, *55*, 2737–2744. [[CrossRef](#)]
86. Nagaosa, N.; Takimoto, J. Theory of neutral-ionic transition in organic crystals. II. Effect of the intersite Coulomb interaction. *J. Phys. Soc. Jpn.* **1986**, *55*, 2745–2753. [[CrossRef](#)]
87. Nagaosa, N. Theory of neutral-ionic transition in organic crystals. III. Effect of the electron-lattice interaction. *J. Phys. Soc. Jpn.* **1986**, *55*, 2754–2764. [[CrossRef](#)]
88. Nagaosa, N. Theory of neutral-ionic transition in organic crystals. IV. Phenomenological viewpoint. *J. Phys. Soc. Jpn.* **1986**, *55*, 3488–3497. [[CrossRef](#)]
89. Tokura, Y.; Koshihara, S.; Iwasa, Y.; Okamoto, H.; Komatsu, T.; Koda, T.; Iwasawa, N.; Saito, G. Domain-wall dynamics in organic charge-transfer compounds with one-dimensional ferroelectricity. *Phys. Rev. Lett.* **1989**, *63*, 2405–2408. [[CrossRef](#)] [[PubMed](#)]
90. Morimoto, T.; Miyamoto, T.; Yamakawa, H.; Terashige, T.; Ono, T.; Kida, N.; Okamoto, H. Terahertz-field-induced large macroscopic polarization and domain-wall dynamics in an organic molecular dielectric. *Phys. Rev. Lett.* **2017**, *118*, 107602. [[CrossRef](#)] [[PubMed](#)]
91. Okimoto, Y.; Horiuchi, S.; Saitoh, E.; Kumai, R.; Tokura, Y. Far-infrared optical response of neutral-ionic phase transition in an organic charge-transfer complex. *Phys. Rev. Lett.* **2001**, *87*, 187401. [[CrossRef](#)]
92. D'Avino, G.; Girlando, A.; Painelli, A.; Lemée-Cailleau, M.H.; Soos, Z.G. Anomalous dispersion of optical phonons at the neutral-ionic transition: Evidence from diffuse X-ray scattering. *Phys. Rev. Lett.* **2007**, *99*, 156407. [[CrossRef](#)] [[PubMed](#)]
93. Masino, M.; Girlando, A.; Soos, Z.G. Evidence for a soft mode in the temperature induced neutral-ionic transition of TTF-CA. *Chem. Phys. Lett.* **2003**, *369*, 428–433. [[CrossRef](#)]
94. Moreac, A.; Girard, A.; Delugeard, Y.; Marqueton, Y. The neutral-to-ionic phase transition of TTF-CA: A Raman and infrared study versus temperature at atmospheric pressure. *J. Phys. Condens. Matter* **1996**, *8*, 3553–3567. [[CrossRef](#)]
95. Masino, M.; Girlando, A.; Brillante, A.; Della Valle, R.G.; Venuti, E.; Drichko, N.; Dressel, M. Lattice dynamics of TTF-CA across the neutral-ionic transition. *Chem. Phys.* **2006**, *325*, 71–77. [[CrossRef](#)]
96. Girlando, A.; Masino, M.; Painelli, A.; Drichko, N.; Dressel, M.; Brillante, A.; Della Valle, R.G.; Venuti, E. Direct evidence of overdamped Peierls-coupled modes in the temperature-induced phase transition in tetrathiafulvalene-chloranil. *Phys. Rev. B* **2008**, *78*, 045103. [[CrossRef](#)]
97. Aubry, S. A unified approach to the interpretation of displacive and order-disorder systems. I. Thermodynamical aspect. *J. Chem. Phys.* **1975**, *62*, 3217–3229. [[CrossRef](#)]
98. Aubry, S. A unified approach to the interpretation of displacive and order-disorder systems. II. Displacive systems. *J. Chem. Phys.* **1976**, *64*, 3392–3402. [[CrossRef](#)]
99. Luty, T.; Cailleau, H.; Koshihara, S.; Collet, E.; Takesada, M.; Lemee-Cailleau, M.H.; Buron-Le Cointe, M.; Nagaosa, N.; Tokura, Y.; Zienkiewicz, E.; et al. Static and dynamic order of cooperative multi-electron transfer. *Europhys. Lett.* **2002**, *59*, 619–625. [[CrossRef](#)]

100. Okamoto, H.; Mitani, T.; Tokura, Y.; Koshihara, S.; Komatsu, T.; Iwasa, Y.; Koda, T.; Saito, G. Anomalous dielectric response in tetrathiafulvalene-*p*-chloranil as observed in temperature- and pressure-induced neutral-to-ionic phase transition. *Phys. Rev. B* **1991**, *43*, 8224–8232. [[CrossRef](#)]
101. Mitani, T.; Kaneko, Y.; Tanuma, S.; Tokura, Y.; Koda, T.; Saito, G. Electric conductivity and phase diagram of a mixed-stack charge-transfer crystal: Tetrathiafulvalene-*p*-chloranil. *Phys. Rev. B* **1987**, *35*, 427–429. [[CrossRef](#)]
102. Tokura, Y.; Okamoto, H.; Koda, T.; Mitani, T. Pressure-induced neutral-to-ionic phase transition in TTF-*p*-chloranil studied by infrared vibrational spectroscopy. *Solid State Commun.* **1986**, *57*, 607–610. [[CrossRef](#)]
103. Kaneko, Y.; Tanuma, S.; Tokura, Y.; Koda, T.; Mitani, T.; Saito, G. Optical reflectivity spectra of the mixed-stack organic charge-transfer crystal tetrathiafulvalene-*p*-chloranil under hydrostatic pressure. *Phys. Rev. B* **1987**, *35*, 8024–8029. [[CrossRef](#)]
104. Takaoka, K.; Kaneko, Y.; Okamoto, H.; Tokura, Y.; Koda, T.; Mitani, T.; Saito, G. Infrared molecular-vibration spectra of tetrathiafulvalene-chloranil crystal at low temperature and high pressure. *Phys. Rev. B* **1987**, *36*, 3884–3887. [[CrossRef](#)]
105. Okamoto, H.; Koda, T.; Tokura, Y.; Mitani, T.; Saito, G. Pressure-induced neutral-to-ionic phase transition in charge-transfer crystals of tetrathiafulvalene-*p*-benzoquinone derivatives. *Phys. Rev. B* **1989**, *39*, 10693–10701. [[CrossRef](#)]
106. Matsuzaki, H.; Takamatsu, H.; Kishida, H.; Okamoto, H. Valence fluctuation and domain-wall dynamics in pressure-induced neutral-to-ionic phase transition of organic charge-transfer crystal. *J. Phys. Soc. Jpn.* **2005**, *74*, 2925–2929. [[CrossRef](#)]
107. Masino, M.; Girlando, A.; Brillante, A. Intermediate regime in pressure-induced neutral-ionic transition in tetrathiafulvalene-chloranil. *Phys. Rev. B* **2007**, *76*, 064114. [[CrossRef](#)]
108. Deng, A.; Beyer, R.; Peterseim, T.; Ivek, T.; Untereiner, G.; Dressel, M. Evolution of ferroelectricity in tetrathiafulvalene-*p*-chloranil as a function of pressure and temperature. *J. Chem. Phys.* **2014**, *140*, 244511. [[CrossRef](#)] [[PubMed](#)]
109. Takehara, R.; Miyagawa, K.; Kanoda, K.; Miyamoto, T.; Matsuzaki, H.; Okamoto, H.; Taniguchi, H.; Matsubayashi, K.; Uwatoko, Y. Electron transport in TTF-CA under high pressures. *Phys. B* **2015**, *460*, 83–87. [[CrossRef](#)]
110. Tsuchiizu, M.; Yoshioka, H.; Seo, H. Phase competition, Solitons, and domain walls in neutral-ionic transition systems. *J. Phys. Soc. Jpn.* **2016**, *85*, 104705. [[CrossRef](#)]
111. Fukuyama, H.; Ogata, M. Solitons in the crossover between band insulator and Mott insulator: Applications to TTF-Chloranil under pressure. *J. Phys. Soc. Jpn.* **2016**, *85*, 023702. [[CrossRef](#)]
112. Mitani, T.; Saito, G.; Tokura, Y.; Koda, T. Soliton formation at the neutral-to-ionic phase transition in the mixed-stack charge-transfer crystal tetrathiafulvalene-*p*-chloranil. *Phys. Rev. Lett.* **1984**, *53*, 842–845. [[CrossRef](#)]
113. Yoshinari, Y.; Maniwa, Y.; Takahashi, T.; Mizoguchi, K.; Mitani, T. ¹H-NMR studies of neutral-ionic transition in TTF-chloranil. *Synth. Met.* **1987**, *19*, 521–526. [[CrossRef](#)]
114. Toudic, B.; Gallier, J.; Boumaza, M.; Cailleau, H. Proton spin-lattice relaxation study of the neutral-to-ionic transition in TTF-chloranil. *J. Phys.* **1990**, *51*, 1671–1678. [[CrossRef](#)]
115. Horiuchi, S.; Tokura, Y. Organic ferroelectrics. *Nat. Mater.* **2008**, *7*, 357–366. [[CrossRef](#)] [[PubMed](#)]
116. Horiuchi, S.; Kobayashi, K.; Kumai, R.; Ishibashi, S. Ionic versus electronic ferroelectricity in donor-acceptor molecular sequences. *Chem. Lett.* **2014**, *43*, 26–35. [[CrossRef](#)]
117. Ishihara, S. Electronic ferroelectricity in molecular organic crystals. *J. Phys. Condens. Matter* **2014**, *26*, 493201. [[CrossRef](#)] [[PubMed](#)]
118. Tomic, S.; Dressel, M. Ferroelectricity in molecular solids: A review of electrodynamic properties. *Rep. Prog. Phys.* **2015**, *78*, 096501. [[CrossRef](#)] [[PubMed](#)]
119. Kagawa, F.; Horiuchi, S.; Matsui, H.; Kumai, R.; Onose, Y.; Hasegawa, T.; Tokura, Y. Electric-field control of solitons in a ferroelectric organic charge-transfer salt. *Phys. Rev. Lett.* **2010**, *104*, 227602. [[CrossRef](#)] [[PubMed](#)]
120. Kagawa, F.; Horiuchi, S.; Tokura, Y. Quantum phenomena emerging near a ferroelectric critical point in a donor-acceptor organic charge-transfer complex. *Crystals* **2017**, *7*, 106. [[CrossRef](#)]
121. Moritomo, T.; Miyamoto, T.; Okamoto, H. Ultrafast electron and molecular dynamics in photoinduced and electric-field-induced neutral-ionic transitions. *Crystals* **2017**, *7*, 132.

122. Nasu, K. (Ed.) *Photoinduced Phase Transitions*; World Scientific: Singapore, 2004.
123. Cailleau, H.; Luty, T.; Koshihara, S.; Servol, M.; Lorenc, M.; Buron-Le Cointe, M.; Collet, E. PIPT from the beginning to future. *Acta Phys. Pol. A* **2012**, *121*, 297–306. [[CrossRef](#)]
124. Cailleau, H.; Lorenc, M.; Buron-Le Cointe, M.; Servol, M.; Cammarata, M.; Collet, E. Impacting materials by light and seeing their structural dynamics. *Eur. Phys. J. Spec. Top.* **2013**, *222*, 1077–1092. [[CrossRef](#)]
125. Tokura, Y.; Okamoto, H.; Koda, T.; Mitani, T.; Saito, G. Nonlinear electric transport and switching phenomenon in the mixed-stack charge-transfer crystal of tetrathiafulvalene-*p*-chloranil. *Phys. Rev. B* **1988**, *38*, 2215–2218. [[CrossRef](#)]
126. Kampfrath, T.; Tanaka, K.; Nelson, K.A. Resonant and nonresonant control over matter and light by intense terahertz transients. *Nat. Photonics* **2013**, *7*, 680–690. [[CrossRef](#)]
127. Hirori, H.; Tanaka, K. Dynamical nonlinear interactions of solids with strong terahertz pulses. *J. Phys. Soc. Jpn.* **2016**, *85*, 082001. [[CrossRef](#)]
128. Koshihara, S.; Takahashi, Y.; Sakai, H.; Tokura, Y.; Luty, T. Photoinduced cooperative charge transfer in low-dimensional organic crystals. *J. Phys. Chem. B* **1999**, *103*, 2592–2600. [[CrossRef](#)]
129. Suzuki, T.; Sakamaki, T.; Tanimura, K.; Koshihara, S.; Tokura, Y. Ionic-to-neutral phase transformation induced by photoexcitation of the charge-transfer band in tetrathiafulvalene-*p*-chloranil crystals. *Phys. Rev. B* **1999**, *60*, 6191–6193. [[CrossRef](#)]
130. Iwai, S.; Tanaka, S.; Fujinuma, K.; Kishida, H.; Okamoto, H.; Tokura, Y. Ultrafast optical switching from an ionic to a neutral state in tetrathiafulvalene-*p*-chloranil (TTF-CA) observed in femtosecond reflection spectroscopy. *Phys. Rev. Lett.* **2002**, *88*, 057402. [[CrossRef](#)] [[PubMed](#)]
131. Tanimura, K. Femtosecond time-resolved reflection spectroscopy of photoinduced ionic-neutral phase transition in TTF-CA crystals. *Phys. Rev. B* **2004**, *70*, 144112. [[CrossRef](#)]
132. Okamoto, H.; Ishige, Y.; Tanaka, S.; Kishida, H.; Iwai, S.; Tokura, Y. Photoinduced phase transition in tetrathiafulvalene-*p*-chloranil observed in femtosecond reflection spectroscopy. *Phys. Rev. B* **2004**, *70*, 165202. [[CrossRef](#)]
133. Iwai, S.; Ishige, Y.; Tanaka, S.; Okamoto, Y.; Tokura, Y.; Okamoto, H. Coherent control of charge and lattice dynamics in a photoinduced neutral-to-ionic transition of a charge-transfer compound. *Phys. Rev. Lett.* **2006**, *96*, 057403. [[CrossRef](#)] [[PubMed](#)]
134. Uemura, H.; Okamoto, H. Direct detection of the ultrafast response of charges and molecules in the photoinduced neutral-to-ionic transition of the organic tetrathiafulvalene-*p*-chloranil solid. *Phys. Rev. Lett.* **2010**, *105*, 258302. [[CrossRef](#)] [[PubMed](#)]
135. Miyamoto, T.; Uemura, H.; Okamoto, H. Role of Coulomb interactions and spin-Peierls dimerizations in neutral-to-ionic phase transition investigated by femtosecond reflection spectroscopy. *J. Phys. Soc. Jpn.* **2012**, *81*, 073703. [[CrossRef](#)]
136. Matsubara, Y.; Okamoto, Y.; Yoshida, T.; Ishikawa, T.; Koshihara, S.; Onda, K. Photoinduced neutral-to-ionic phase transition in tetrathiafulvalene-*p*-chloranil studied by time-resolved vibrational spectroscopy. *J. Phys. Soc. Jpn.* **2011**, *80*, 124711. [[CrossRef](#)]
137. Itoh, C.; Fukuda, S. FT-IR study of Photo-induced phase transition in organic charge-transfer crystal of TTF-CA. *Phys. Status Solidi* **2006**, *3*, 3446–3451. [[CrossRef](#)]
138. Collet, E.; Lemée-Cailleau, M.H.; Buron-Le Cointe, M.; Cailleau, H.; Wulff, M.; Luty, T.; Koshihara, S.; Meyer, M.; Toupet, L.; Rabiller, P.; et al. Laser-induced ferroelectric structural order in an organic charge-transfer crystal. *Science* **2003**, *300*, 612–615. [[CrossRef](#)] [[PubMed](#)]
139. Guerin, L.; Collet, E.; Lemée-Cailleau, M.H.; Buron-Le Cointe, M.; Cailleau, H.; Plech, A.; Wulff, M.; Koshihara, S.; Luty, T. Probing photoinduced phase transition in a charge-transfer molecular crystal by 100 picosecond X-ray diffraction. *Chem. Phys.* **2004**, *299*, 163–170. [[CrossRef](#)]
140. Collet, E.; Buron-Le Cointe, M.; Cailleau, H. X-ray diffraction investigation of the nature and the mechanism of photoinduced phase transition in molecular materials. *J. Phys. Soc. Jpn.* **2006**, *75*, 011002. [[CrossRef](#)]
141. Nowaza, S.; Adachi, S.; Takahashi, J.I.; Tazaki, R.; Guerin, L.; Daimon, M.; Tomita, A.; Sato, T.; Chollet, M.; Collet, E.; et al. Developing 100 ps-resolved X-ray structural analysis capabilities on beamline NW14A at the Photo Factory Advanced Ring. *J. Synchrotron Radiat.* **2007**, *14*, 313–319. [[CrossRef](#)] [[PubMed](#)]
142. Guerin, L.; Hebert, J.; Buron-Le Cointe, M.; Adachi, S.; Koshihara, S.; Cailleau, H.; Collet, E. Capturing one-dimensional precursors of a photoinduced transformation in a material. *Phys. Rev. Lett.* **2010**, *105*, 246101. [[CrossRef](#)] [[PubMed](#)]

143. Hoshino, M.; Nozawa, S.; Sato, T.; Tomita, A.; Adachi, S.; Koshihara, S. Time-resolved X-ray crystal structure analysis for elucidating the hidden “over-neutralized” phase of TTF-CA. *RSC Adv.* **2013**, *3*, 16313–16317. [[CrossRef](#)]
144. Bertoni, R.; Lorenc, M.; Cailleau, H.; Tissot, A.; Laisney, J.; Boillot, M.L.; Stoleriu, L.; Enaschescu, C.; Collet, E. Elastically driven cooperative response of a molecular material impacted by a laser pulse. *Nat. Mater.* **2016**, *15*, 606–610. [[CrossRef](#)] [[PubMed](#)]
145. Lorenc, M.; Hebert, J.; Moisan, N.; Trzop, E.; Servol, M.; Buron-Le Cointe, M.; Cailleau, H.; Boillot, M.L.; Pontecorvo, E.; Wulff, M.; et al. Successive dynamical steps of photoinduced switching of a molecular Fe(III) spin-crossover material by time-resolved X-ray diffraction. *Phys. Rev. Lett.* **2009**, *103*, 028301. [[CrossRef](#)] [[PubMed](#)]
146. Peterseim, T.; Haremski, P.; Dressel, M. Random-walk annihilation process of photo-induced neutral-ionic domain walls in TTF-CA. *Europhys. Lett.* **2015**, *109*, 67003. [[CrossRef](#)]
147. Peterseim, T.; Dressel, M. Molecular dynamics of electrical- and optical-driven phase transitions: Time-resolved infrared studies using Fourier-transform spectrometers. *J. Infrared Millim. Terahz Waves* **2017**, *38*, 104–123. [[CrossRef](#)]
148. Miyamoto, T.; Yada, H.; Yamakawa, H.; Okamoto, H. Ultrafast modulation of polarization amplitude by terahertz fields in electronic-type organic ferroelectrics. *Nat. Commun.* **2013**, *4*, 2586. [[CrossRef](#)] [[PubMed](#)]
149. Gomi, H.; Yamagishi, N.; Mase, T.; Inagaki, T.J.; Takahashi, A. Instantaneous charge and dielectric response to terahertz pulse excitation in TTF-CA. *Phys. Rev. B* **2017**, *95*, 094116. [[CrossRef](#)]
150. Ishikawa, T.; Sagae, Y.; Naitoh, Y.; Kawakami, Y.; Itoh, H.; Yamamoto, K.; Yakushi, K.; Kishida, H.; Sasaki, T.; Ishihara, S.; et al. Optical freezing of charge motion in an organic conductor. *Nat. Commun.* **2014**, *5*, 5528. [[CrossRef](#)] [[PubMed](#)]
151. Yonemitsu, K.; Nasu, K. Theory of photoinduced phase transitions. *J. Phys. Soc. Jpn.* **2006**, *75*, 011008. [[CrossRef](#)]
152. Yonemitsu, K.; Nasu, K. Theory of photoinduced phase transitions in itinerant electron systems. *Phys. Rep.* **2008**, *465*, 1–60. [[CrossRef](#)]
153. Huai, P.; Zheng, H.; Nasu, K. Theory for photoinduced ionic-neutral structural phase transition in quasi-one-dimensional organic molecular crystal TTF-CA. *J. Phys. Soc. Jpn.* **2000**, *69*, 1788–1800. [[CrossRef](#)]
154. Yonemitsu, K. Phase transition in a one-dimensional extended Peierls-Hubbard model with a pulse of oscillating electric field: II linear behavior in neutral-to-ionic phase transition. *J. Phys. Soc. Jpn.* **2004**, *73*, 2879–2886. [[CrossRef](#)]
155. Yonemitsu, K. Interchain coupling effects on photoinduced phase transitions between neutral and ionic phases in an extended Hubbard model with alternating potentials and an electron-lattice coupling. *Phys. Rev. B* **2006**, *73*, 155120. [[CrossRef](#)]
156. Yonemitsu, K. Effects of lattice and molecular phonons on photoinduced neutral-to-ionic transition dynamics in tetrathiafulvalene-*p*-chloranil. *J. Phys. Soc. Jpn.* **2011**, *80*, 084707. [[CrossRef](#)]
157. Cavatorta, L.; Painelli, A.; Soos, Z.G. Coherent excitations at the neutral-ionic transition: Femtosecond dynamics on diabatic potential energy surfaces. *Phys. Rev. B* **2015**, *91*, 174301. [[CrossRef](#)]
158. Brazovskii, S.; Kirova, N. Dynamical phase transitions and pattern formation induced by a pulse pumping of excitons to a system near a thermodynamic instability. *Phys. Rev. B* **2016**, *94*, 054302. [[CrossRef](#)]
159. Landau, L.D.; Lifshitz, E.M. Statistical Physics. In *Course of Theoretical Physics*, 3rd ed.; Pergamon Press: Oxford, UK, 2008; Volume 5, pp. 459–471.

